International Journal of Disaster Risk Reduction 130 (2025) 105810

Contents lists available at ScienceDirect

International Journal of Disaster Risk Reduction

journal homepage: www.elsevier.com/locate/ijdrr

A systemic approach to complex landslide risk reduction in coastal tourist areas: The case of Sirolo, central Italy

Elisa Mammoliti [a,*], Eleonora Gioia [b,**], Davide Fronzi [a], Adriano Mancini [c], Giorgio Mattioli [a], Roberta Bonì [d], Fabrizio Pontoni [e], Stefano Marabini [f], Stefano Mazzoli [g], Alberto Tazioli [a], Alessandra Negri [b]

[a] Department of Science and Engineering of Matter, Environment and Urban Planning (SIMAU), Università Politecnica delle Marche, Ancona, Italy
[b] Department of Life and Environmental Sciences (DISVA), Università Politecnica delle Marche, Ancona, Italy
[c] Department of Information Engineering (DII), Università Politecnica delle Marche, Ancona, Italy
[d] Department of Science, Technology and Society (STS), University School for Advanced Studies (IUSS), Pavia, Italy
[e] Geoequipe Associated Technical Studio, Via Sandro Pertini 55, 62029, Tolentino (MC), Italy
[f] Independent Researcher, Via San Martino 1, Faenza (RA), Italy
[g] School of Science and Technology, Geology Section, University of Camerino, Camerino, Italy

ARTICLE INFO

Keywords:
Complex landslides
Footslope processes
Risk perception
Deep learning modeling
Risk management

ABSTRACT

Coastal landslides in structurally complex and tourist-rich areas, such as the Monte Conero promontory in central Italy, pose significant challenges to environmental stability and public safety. In these settings, complex landslides often involve deep-seated translational movements evolving into sudden debris collapses at the footslope, generating significant hazards in beach areas heavily frequented by tourists. This study develops a conceptual, transferable model for complex landslide behavior in the Sirolo coastal sector in an integrated Hazard–Exposure–Vulnerability framework. The hazard component is investigated by systematically integrating multi-source data, including COSMO-SkyMed and Sentinel-1 Differential Interferometric Synthetic Aperture Radar (DInSAR) data, *in-situ* inclinometer and piezometric time series, and high-resolution geological and geomorphological field mapping. Rainfall analyses and an Extreme Rainfall Periodic Index (ERPI) were used to explore the correlation between precipitation distribution and kinematic responses of the slope, offering an empirical insight into seasonal hazard modulation. To assess exposure, we developed a deep learning model to estimate beach attendance using limited Google Earth imagery (5 useable acquisition dates, moderate resolution), calibrated with regional tourism statistics, enabling a spatially and temporally explicit assessment of human presence. Finally, to explore vulnerability, a face-to-face survey was carried out to document gaps in visitor awareness of risk and civil-protection procedures. This integrated approach offers enhanced predictive capacity and supports targeted mitigation and communication measures in coastal environments characterized by complex landslides and intense seasonal human activity. To the authors knowledge, this is the first study integrating geological monitoring, rainfall indices, satellite data, deep learning-based exposure, and tourist risk perception into a systemic coastal landslide risk framework.

* Corresponding author.
** Corresponding author.
E-mail addresses: e.mammoliti@staff.univpm.it (E. Mammoliti), e.gioia@staff.univpm.it (E. Gioia).

https://doi.org/10.1016/j.ijdrr.2025.105810
Received 15 July 2025; Received in revised form 7 September 2025; Accepted 7 September 2025
Available online 11 September 2025

1. Introduction

Coastal landslides in tourist-rich regions pose a significant threat to both environmental integrity and societal safety, especially when they exhibit a complex behaviour that combines deep-seated translational movements and rapid debris failures [1,2]. Coastal slope processes may evolve either into paroxysmal and catastrophic events [3], and/or exhibit a persistent, slow deformation regime [4–6]. In coastal environments, landslide susceptibility is strongly influenced by the interplay between cliff rheology and the litho-structural framework, as well as by external forcing factors, such as intense rainfall, seismic activity, storm-induced wave loading and sea-level fluctuation [7]. In this regard, the role of footslope processes in complex landslides is increasingly recognized as a key component in understanding slope failure evolution, especially in multi-stage events common to structurally complex terrains such as the Apennines. The toe, or footslope zone, does not simply act as a passive depositional area but actively interacts with the main landslide body through both mechanical and hydrological coupling. For instance, Cotecchia et al. [8] illustrate how fissured clay-rich terrains exhibit weakening and increased permeability at the footslope due to creeping deformation and fracturing, emphasizing that atmospheric, vegetation, and rainfall interactions influence pore pressure variations down to deep layers, confirming footslope involvement in deep-seated slope movements [9]. In many cases, this segment of the slope becomes the first to fail due to the combination of stress transfer from the upper slide mass and its own morphological and hydrogeological vulnerability. Moreover, in coastal settings, footslope sectors are often subjected to additional destabilizing forces induced by marine erosion, which can progressively undercut the slope toe, reduce basal support, and thereby enhance the likelihood of collapse even in the absence of active movement in the upper landslide body. As shown by Chen et al. [10], infiltration from upper-slope runoff into the lower slope can significantly lower the Factor of Safety in the toe area, particularly when combined with delayed pore pressure dissipation. This phenomenon is often observed even in the absence of active movement in the upper mass, indicating a potential for localized footslope failures to act as precursors to larger-scale mobilization. Studies such as those by Luino and De Graff [11], show that the evolution from deep-seated sliding to footslope debris collapse follows a predictable progression, wherein load transfer and strain accumulation in the toe ultimately exceed its strength threshold, producing abrupt detachment and rapid downslope motion. Such toe failures, in turn, feed back into the main landslide system, contributing to episodic accelerations or reactivations. Furthermore, hydrogeological models of complex landslides with dual aquifer systems, featuring an unconfined aquifer in the slide mass overlying a confined unit, demonstrate that overpressure in the lower unit can initiate failure at the toe, especially along permeability contrasts and lithological discontinuities [12]. The conceptual framework for gravitational slope evolving into translational slides and ultimately cascading into debris-flow or fall at the slope toe is well supported by studies in Italy and beyond [9,10 and references therein]. In such multi-stage failures, hydromechanics plays a key role; research in the northern Apennines shows how dual groundwater units in unconfined, fracture-filled slide body overlaying a confined unit, govern permeability changes and thus influence mobilization of deep translational masses [12, 13]. This insight is particularly relevant in the Mediterranean climate of Conero, where seasonal recharge and fractured carbonate bedrock establish dynamic pore-pressure conditions.This context provides the peculiar setting for a compound risk physically driven by complex slope processes and socially amplified by large, transient, and often unfamiliar visitor populations. Indeed, risk results from the interaction of hazard, exposure, and vulnerability [14]: here, the hazard is the seasonal kinematics that range from slow translational movements to sudden footslope collapses; exposure reflects the daily crowding of beach users in confined coastal strips; and vulnerability stems from the limited knowledge and preparedness among non-resident users. From a behavioural standpoint, people's protective decisions depend not only on threat appraisal but also on response efficacy, self-efficacy, trust, and prior experience [15–17]. Studies focusing on tourist populations confirm gaps in hazard knowledge and evacuation intent in coastal contexts [18,19] and show that disaster-related risk perception shapes travel intentions and compliance with advice [20,21]. Moreover, unlike residents, empirical work in coastal settings shows that tourists frequently under-detect or misinterpret hazard cues and safety signage at beaches and rocky coasts, depressing situational awareness and delaying protective action [22–24]. On rocky coasts specifically, risk management gaps and the need for dedicated frameworks are well documented [25–27]. Accordingly, integrating the tourism sector into emergency-management structures is repeatedly recommended to improve readiness and communication along popular coasts [28].

In the Mediterranean area, seasonal tourism creates pronounced spikes in coastal landslide exposure. This issue is particularly relevant in the Municipality of Sirolo (Marche Region, central Italy), a small coastal town located on the eastern slopes of Monte Conero, overlooking the Adriatic Sea. Despite its limited resident population, approximately 4100 inhabitants according to ISTAT [29], Sirolo is a renowned summer destination. In 2023 alone, it attracted over 55000 tourist arrivals [30], with daily peaks concentrated in the narrow stretch of cliff-backed beaches such as San Michele and Sassi Neri. The strong seasonal influx of non-resident visitors, combined with the morphological sensitivity of the coastal slopes, creates a critical interface between hazard and human exposure. Here, the IFFI project, that is the Inventory of Landslide Phenomena in Italy [31], shows that in the coastline north to Sirolo, complex landslides composed by translational slides evolve into abrupt detachment and collapse of a 10 m thick debris at the footslope, resulting in large trenches and substantial morphological changes. Given the fractured carbonate lithology and seasonal hydrological regime of the Conero promontory, the footslope is not only a zone of morphological change but also a mechanically sensitive component of the landslide system. Its evolution can critically alter the stability of the entire slope, necessitating focused monitoring and modeling to assess both short-term hazard and long-term morphodynamic adjustments. To effectively address both the physical processes governing slope instability and their societal implications, particularly in densely visited coastal areas, we implemented a multi-disciplinary approach that integrates: (i) multi-sensor satellite-based Differential Interferometry Synthetic Aperture Radar (DInSAR) time series; (ii) in-situ monitoring (inclinometers and piezometers); (iii) high-resolution geomorphological and structural field surveys to map surface evidence of instability; (iv) rainfall trend analysis using the Extreme Rainfall Periodicity

Index (ERPI); (v) dynamic exposure estimates derived from image-based deep-learning counts of beach users, calibrated against official tourism statistics; and (vi) an on-site survey of visitor risk perception administered during the peak season. Rainfall analyses, supported by the evaluation of an ERPI, were incorporated into the study to investigate the potential correlation between precipitation distribution along the years and the slope kinematics. These analyses provided crucial inputs for the development of a site-specific conceptual model, enhancing the understanding of seasonal triggering conditions and their role in controlling the transition from slow deformation to sudden failure. Central to our approach is the development of a deep learning model designed to estimate seasonal tourist presence based on image-derived data, which was subsequently calibrated and cross-validated against official regional tourism statistics. This exposure model enables a spatio-temporally explicit representation of population distribution along the beach, offering critical insight into the temporal overlap between hazard occurrence and human presence.

These data streams are synthesized into a site-specific conceptual model that highlights the seasonal modulation of slope activity and its implications for landslide hazard. Fig. 1 illustrates the conceptual integration framework implemented in this study, showing how landslide phenomenological knowledge informs risk evaluation and management through exposure and vulnerability assessments. The framework is structured around three interconnected spheres (hazard, exposure and vulnerability, and risk) providing a comprehensive understanding of geological hazards and a practical tool for local authorities and public agencies. This approach accounts for both permanent and transient populations, such as tourists visiting coastal areas. Each sphere employs a multi-method approach. Hazard assessment combines rainfall trend analysis (ERPI), geological and hydrogeological monitoring, and remote sensing of surface processes. This data feeds into slope dynamics and collapse predictions. Exposure and vulnerability integrate human factors, including beach-occupancy (estimated via deep learning) and tourist risk perception (collected through on-site surveys). Together, these components form an integrated systemic risk assessment, establishing a robust knowledge base to support informed coastal landslide risk management.

As previously mentioned, while individual components of this problem, such as landslide monitoring, rainfall trend analysis, exposure estimation from imagery, and tourist risk-perception surveys, have been explored in prior studies, they are rarely integrated into a single, decision-oriented framework tailored to tourist beaches affected by complex landslides [25,32,33]. To the best of our knowledge, no previous studies have jointly integrated geological and hydrogeological modelling, remote sensing data, deep learning methods, and on-site tourist risk perception analysis in a Mediterranean coastal landslide context. Our contribution is to operationalize this integration for the Sirolo sector of Monte Conero, a Mediterranean coastal hotspot where climate change is expected to intensify extreme rainfall and associated slope instabilities [34], in order to support Disaster Risk Reduction (DRR) and risk communication. The workflow links process-based hazard understanding with dynamic exposure and visitor behavior, yielding a decision-oriented framework that informs targeted measures (e.g., signage and access management, seasonal monitoring priorities, and focused public messaging). Although tailored to Sirolo, the design is modular and data-independent, making it readily transferable to other

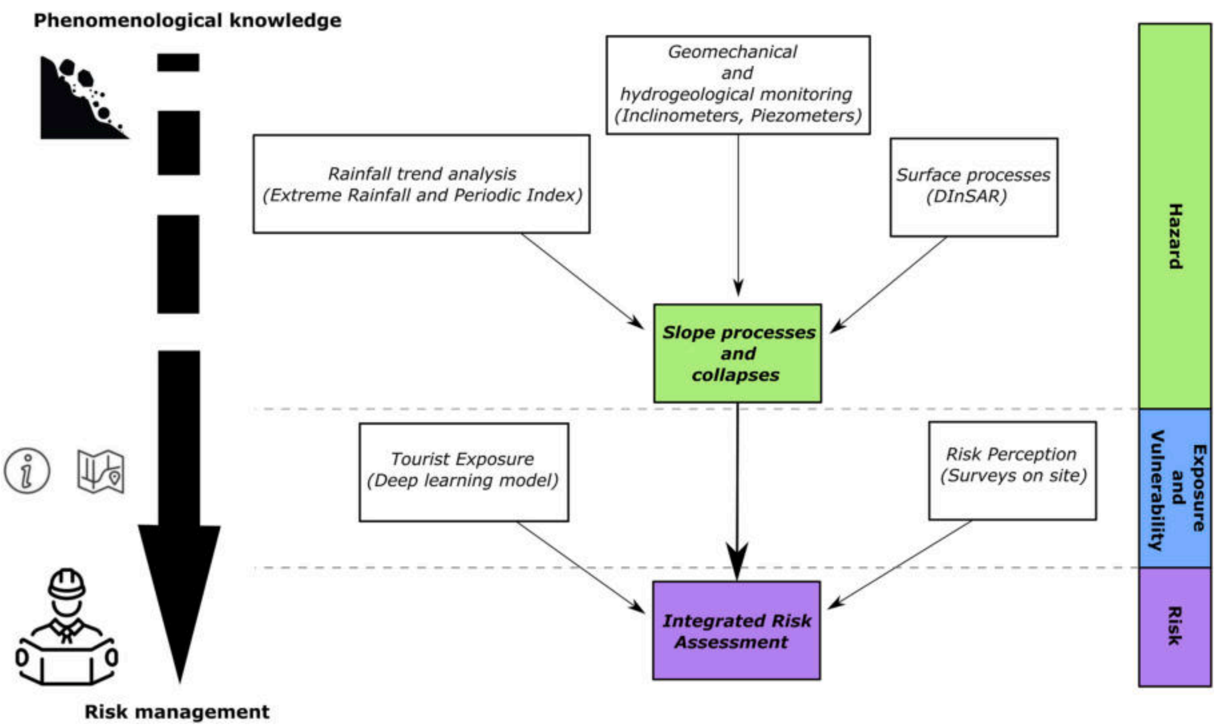

Fig. 1. Conceptual diagram showing how the systemic integration framework for landslide risk was implemented in this study. The framework links Hazard (rainfall trends, monitoring, remote sensing) with Exposure & Vulnerability (deep-learning exposure estimates, visitor risk perception) to support Risk evaluation and mitigation actions.

cliff-backed beaches with comparable geomorphological and touristic conditions. In a region widely recognized as a climate-change hotspot [35,36] such integrated hazard–exposure–risk frameworks are increasingly relevant for anticipating toe-collapse windows and underpinning site-specific mitigation strategies in seasonally crowded coastal environments.

2. Geological setting and structural features of the area

The Monte Conero is primarily characterized by an active cliff, the morphology of which is intimately linked to the structural and lithologic features of the bedrock. It represents the emerged part of an imbricate fan of west-dipping thrusts, which constitute the outermost portion of the Apennine fold and thrust belt.

Tectonic deformation associated with the Apennine orogenesis led to the emergence of the promontory starting from the Early Pleistocene [37], causing folding and fracturing of the sedimentary rocks occurring in the area. The Monte Conero structure is an anticline with a NNE trending fold axis. The southern sector of the Monte Conero anticline consists of an ENE-verging, inclined to overturned fold. Its western limb dips gently to the WSW, whereas the eastern limb is steep to vertical, to locally overturned. To the north, NE-SW striking faults separate the main anticline from adjacent minor folds and thrusts, including a westward

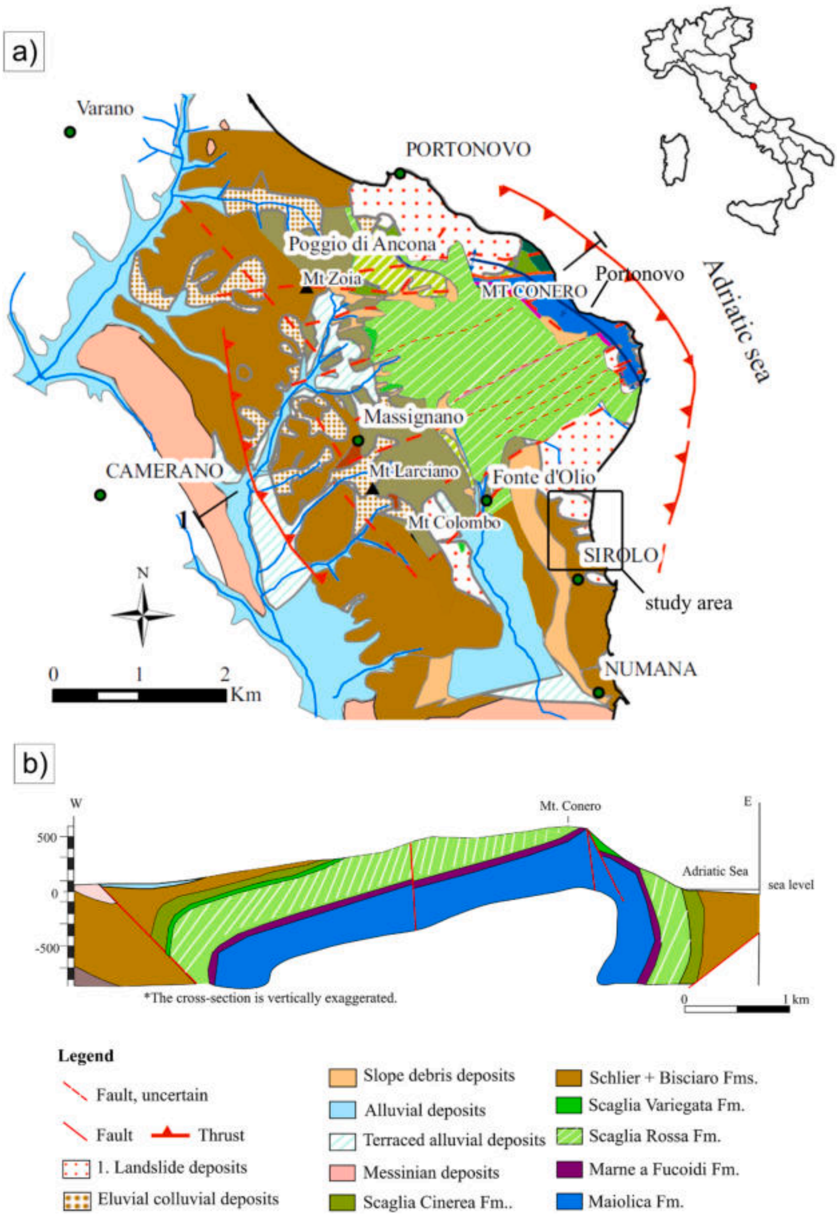

Fig. 2. a) Geological map of the Monte Conero with indication of the study area b) geological cross-section (modified from Ref. [41]).

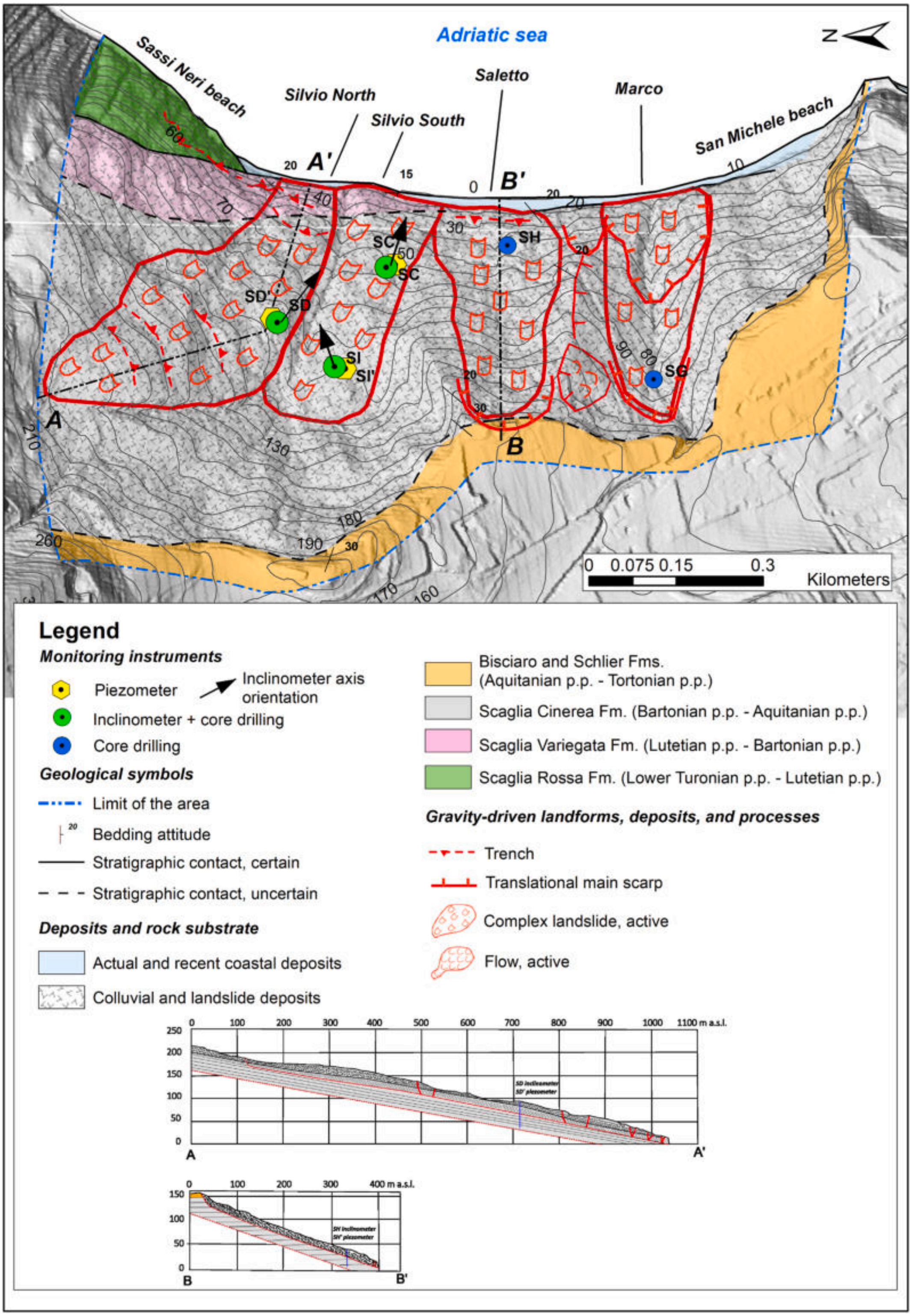

Fig. 3. Geological map of the study area with the monitoring layout and interpretative schematic geological sections.

anticlinal-synclinal pair offset by NW-SE trending minor discontinuities (Fig. 2). These minor discontinuities include both reverse and strike-slip faults, such as the E-W trending fault near Fosso Fontanaccia (west of Portonovo, Fig. 2) and several N-S or NE-SW striking faults that influenced valley formation in the region [38]. In some areas, these fault sets delineate the boundary between carbonate-dominated formations to the south and marly Miocene units to the north (from the Bisciaro-Schlier Formation to lower Pliocene marls and sands). The Miocene units are deformed into minor folds and thrusts with ENE vergence, consistent with the regional shortening. Recent tectonic activity affecting the Monte Conero ridge since the early Pleistocene [39,40] modified the previous fold-thrust belt tectonic setting. The related faults mostly display minor displacements.

The Tithonian to Aptian Maiolica limestones, exposed in the core of the asymmetrical Monte Conero anticline and offset by E-W striking faults, represent the oldest outcropping rocks along the coastal area of the Marche region). Numerous authors have also highlighted the presence of pre-orogenic structures at both mesoscale and regional scale [40,42,43]. Synsedimentary faults can be assumed as the responsible for the differences in the lithological terms of the Umbria-Marche succession. In fact, here the almost complete stratigraphic Umbria-Marche succession (Auctt.) overlying the Maiolica Formation (Fm.) includes the Marne a Fucoidi Fm.

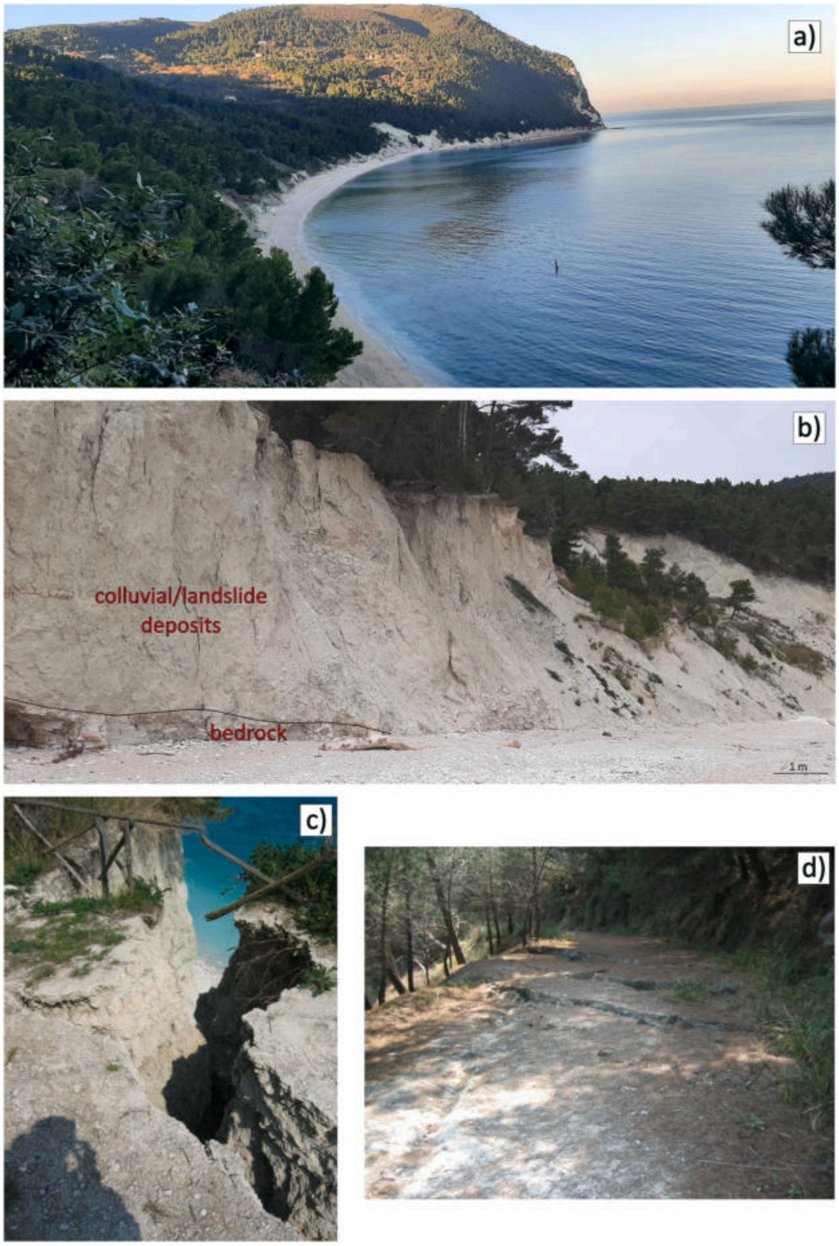

Fig. 4. a) Near-vertical cliff showing the contact between the eluvial-colluvial cover and the underlying bedrock, with clear signs of toe erosion due to marine action. b) and c) Deep tensile crack along the cliff edge, indicating active displacement and potential toppling or sliding mechanisms.

(that is considerably thinner than that generally observed elsewhere in the Umbria-Marche Apennines), while both the Scaglia Bianca Fm. and the Bonarelli level are missing [38]. The Marne a Fucoidi Fm. are directly overlain by the Scaglia Rossa Fm., which passes to the Scaglia Variegata. The stratigraphically overlying Scaglia Cinerea, showing a thickness of about 40 m, characterizes the cliff of the San Michele - Sassi Neri beach. Above these formations, the marly units of the Bisciaro and Schlier Fm. and extensive Quaternary deposits, including detrital, alluvial, and colluvial materials, are present.

All these tectonic and lithostratigraphic features played a key role in shaping the relief, influenced by varying climatic conditions, and have significantly impacted the evolution of the Monte Conero ridge, particularly through the erosive force of the sea and the effect of gravity.

3. Landslides characteristics and geomechanical data

The Monte Conero coastal area, located in the Marche Region (central Italy), exhibits widespread landslide activity, involving both rockslides and landslides in loose deposits. These phenomena are particularly concentrated near steep marine cliffs shaped by active erosion. In these zones, slope gradients are most pronounced at lower elevations due to wave action, while upper sections of the slope tend to be gentler, having been modified by surface erosion and fluvial processes [37]. In this study, a detailed geological and geomorphological survey was carried out to identify active and relict landslides at the surface, as well as to characterize the local geology. The results of this survey are summarized in the geological map and related sketch cross-sections (Fig. 3), which illustrate both the stratigraphic setting and the spatial distribution of slope instabilities along the coastal section between Sassi Neri and San Michele beaches (Fig. 4a). In this sector, slope failures are closely linked to the complex geological setting, where tectonically deformed and weathered bedrock is overlain by weak eluvial-colluvial deposits (up to 10 m thick) forming near-vertical cliffs (Fig. 4b), which are particularly susceptible to wave-induced undercutting. The bedrock primarily consists of the Scaglia Cinerea Fm., that has undergone significant tectonic disruption and alteration, resulting in reduced rock mass quality with a Geological Strength Index (GSI) between 25 and 40. Above this, borehole investigations (Fig. 3 and Table 1) have identified a colluvial/landslide deposit layer with variable thickness between 5.3 and 11.4 m, composed of unconsolidated materials with low mechanical strength. Geotechnical laboratory analyses [44] categorize the detrital cover as a silt of low plasticity (ML), based on Atterberg limits plotted on the Casagrande chart. The Scaglia Cinerea Fm. itself comprises finely layered marly limestones and marls, with increasing marl content toward the top. Its mechanical response ranges from that of a weak rock, showing uniaxial compressive strengths between 20 and 25 MPa, that of a granular material when highly weathered or fractured. Degradation of the rock matrix produces fine-grained materials still classifiable as low plasticity silts.

The comparative analysis of boreholes D, C, I, H, and G (Table 1 and Fig. 3) reveals significant stratigraphic and geotechnical variability across the landslide sectors. The colluvial deposits exhibit notable differences in thickness and composition. Boreholes D and I, located at the same elevation, show substantially thicker colluvial layers/landslide deposits (11.4 m and 13.1 m respectively, Fig. 4b), suggesting significant reworking and accumulation of landslide material in these zones. In contrast, Borehole C presents a thinner colluvial cover (5.5 m), composed of heterometric and chaotic materials with low compaction, indicative of more recent and unstable depositional processes. Boreholes G and H also reveal colluvial or landslide-related deposits, with G showing 5.3 m of chaotic material composed of calcarenitic pebbles and marly-limestone gravels in a clayey-silty matrix with brownish fine sands, and H recording 7.2 m of clayey silts with sand and marly gravels, including blocks of marls and calcareous marls, reflecting medium to low compaction conditions.

The underlying weathered bedrock, corresponding to the Scaglia Cinerea Fm., occurs in all boreholes with thicknesses ranging between approximately 6.9 and 11.7 m. High degrees of fracturing and weathering occur in the intervals between approximately 5.5 m and 18.5 m, with very poor rock quality in some zones (RQD = 0 %), especially between 11.4 m and 21.7 m in Borehole D. In Borehole C, the weathered bedrock is characterized by oxidized zones and poor to moderate consistency, while Borehole I reveals a transitional contact marked by a thin, highly fractured yellowish marl layer indicating a shift toward more competent lithologies. In Borehole H, the weathered bedrock (7.8–18.5 m) consists of marls and calcareous marls with moderate weathering and fracturing, including fractured zones at specific depths (14.5, 15.5, 17.3 m). Borehole G weathered section (5.3–9.2 m) shows alternations of marls and weathered calcareous marls with hazelnut color, greenish hues, and yellowish and/or bluish veins, with moderate weathering and a highly fractured zone between 7.9 and 9.2 m. Below the weathered bedrock, the unweathered bedrock interval of the Scaglia Cinerea Fm. extends from depths of approximately 12 m to the bottom of each borehole. This unit displays a high variability in fracturing degree, with RQD values ranging from 0 % to 90 % across all sites. Fracture dips vary widely from subvertical to sub horizontal orientations, affecting rock mass quality. Borehole H shows grey-greenish marly limestones with blackish carbonaceous inclusions interbedded with fractured marls bearing calcite (18.5–30.2 m), exhibiting low fracturing and high RQD values (70–100 %), with bedding dips of about 20°. Borehole G records a thick sequence from 9.2 to 36.0 m of grey-greenish marly limestones with blackish carbonaceous inclusions, with moderate fracturing and highly fractured zones (RQD 60–100 %), including a notably fractured interval between 13.9 and 18.8 m with fractures dipping between 5° and 10° and up to 80°, sometimes filled with silty clays. The co-location of Boreholes D and I at the same elevation allows for reliable stratigraphic correlation, confirming consistency in the thickness of both colluvial and weathered units while highlighting variations in rock fabric, fracturing intensity, and mechanical properties within the deeper bedrock. Inclusion of Boreholes G and H expands the spatial understanding of the stratigraphic framework and geotechnical characteristics, illustrating local heterogeneities in lithology, weathering state, and fracturing patterns that are critical for landslide risk assessment.

From a kinematic perspective, the landslides affecting the area between Sassi Neri and San Michele beaches can be classified as complex landslides. These slope instabilities develop within a thick heterogeneous deposit, generally described as eluvial-colluvial

Table 1
Boreholes interpretation with an overview of stratigraphy, lithology, weathering and rock mass quality.

Stratigraphic Unit	Borehole	Landslide	Depth Interval (m)	Thickness (m)	Lithology	Weathering/ Fracturing	RQD (%)	Notes
Colluvial and landslide deposits	D	Silvio North	0–11.4	11.4	Clayey-silty soils with variable gravel content	–	–	Low consistency
	C	Silvio South	0–5.5	5.5	Chaotic deposit of grey-bluish silty clays and clayey silts with yellowish-brown hues and fine hazel-coloured sands, containing greyish calcareous-marly to marly gravels.	–	–	Low consistency
	I	Silvio South	0–13.1	13.1	Clayey silts with sand and marly gravels	–	–	Medium to high-consolidated
	H	Saletto	0.6–7.8	7.2	Clayey silts with sand and marly gravels with blocks of marls and calcareous marls	–	–	Low to medium compaction
	G	Marco	0–5.3	5.3	Chaotic material composed of calcarenitic pebbles and marly-limestone gravels in a clayey-silty and silty-clayey matrix, with the presence of brownish fine sands	–	–	Medium compaction
Weathered Bedrock	D	Silvio North	11.4–18.3	6.9	Grey to brownish-grey marls and calcareous marls (Scaglia Cinerea Fm.)	Highly fractured, extremely weathered	0 %	Extremely poor rock quality
	C	Silvio South	5.5–12.4	6.9	Grey-bluish marls and calcareous marls, locally oxidized (Scaglia Cinerea Fm.)	Highly weathered, oxidized zones	–	Transitional zone, significant weathering, low consistency
	I	Silvio South	13.1–24.0	10.9	Marls and calcareous marls (Scaglia Cinerea Fm.)	Intensely fractured, variable weathering	20–60 %	Thin yellowish marl at 23.7–24.0 m as transitional layer
	H	Saletto	7.8–18.5	10.7	Marls and calcareous marls (Scaglia Cinerea Fm.)	Moderate weathering	–	Fractured zones at 14.5, 15.5, 17.3 m
	G	Marco	5.3–9.2	3.9	Alternations of marls and weathered calcareous marls, hazelnut in color with greenish hues and yellowish and/or bluish veins (Scaglia Cinerea Fm.)	Moderate weathering	–	Highly fractured zone between 7.9 and 9.2 m
Unweathered Bedrock	D	Silvio North	18.3–28.0	9.3	Marls and calcareous marls (Greyish with greyish and/or yellowish hues and brownish smears on the surfaces) (Scaglia Cinerea Fm.)	Highly fractured, low weathered	0–70 %	Fractures dip angle 15°–45°, bedding 15°. High fractured zone (RQD = 0 %) between 20 and 21.7 m
	D	Silvio North	28.0–31.0	3.0	Vinaceous to greenish-grey marly limestones (Scaglia Variegata Fm.)	Moderate fracturing	30–80 %	Fractures dip 30–70°
	D	Silvio North	31.0–54.5	23.5	Marly limestones interbedded with decimetric levels of greenish-grey marls (Scaglia Cinerea Fm.)	Moderate fracturing	30–80 %	High variability of fracturing degree, fractures dip between 30° and 70°
	C	Silvio South	12.4–20.7	8.3	Compact grey-blue marls and calcareous marls (Scaglia Cinerea Fm.)	Pervasively fractured, structurally heterogeneous	20–70 %, mostly 20–55 %	Poor to moderate rock mass quality

(continued on next page)

Table 1 (*continued*)

Stratigraphic Unit	Borehole	Landslide	Depth Interval (m)	Thickness (m)	Lithology	Weathering/ Fracturing	RQD (%)	Notes
	C	Silvio South	20.7–30.0	9.3	Bluish-grey with greenish shades marly limestones and calcareous marls (Scaglia Cinerea Fm.)	Highly fractured	10–50 %	Poor to moderate rock mass quality
	I	Silvio South	24.0–40.0	16	Interbedded marly limestones and calcareous marls (grey-greenish), fossiliferous (Scaglia Cinerea Fm.)	High variability of fracturing degree	20–90 %, generally high	Bedding dips 10°–15°, increased quality at depth
	H	Saletto	18.5–30.2	11.7	Grey-greenish marly limestones with blackish carbonaceous inclusions, interbedded with occasional levels of fractured marls bearing calcite (Scaglia Cinerea Fm.)	Low fracturing	70–100 %	Bedding dips of approximately 20°
	G	Marco	9.2–12.4	3.2	Marly limestones and calcareous marls of grey-greenish color with blackish carbonaceous inclusions (Scaglia Cinerea Fm.)	Moderate fracturing	60–100 %	Intensely fractured (with dips ranging from subvertical to subhorizontal). In some cases, the fractures are filled with silty clays
	G	Marco	12.4–36.0	23.6	Grey-greenish marly limestones with blackish carbonaceous inclusions; fractured (Scaglia Cinerea Fm.)	Moderate fracturing	60–100 %	Highly fractured zone between 13.9 and 18.8 m. Fractures dips 5°–10° to 80°

material interbedded with relict landslide deposits, which rests upon the bedrock of the Scaglia Cinerea Fm. (Fig. 3). The landslides exhibit a dual kinematic behaviour: in the upper portion of the slope, movement initiates as a translational slide, whereas in the lower sections, it evolves into footslope dynamics dominated by rockfalls. As clearly shown in Fig. 4c and d, deep trenches exceeding 1 m in width are present in the downslope zones (also indicated in Fig. 3). These features represent the morphological expression of the landslide's progressive movement at its toe.

4. Monitoring data

4.1. Subsurface monitoring: evidence from inclinometers and piezometers

Within the study area, three inclinometers have been installed to monitor ground displacements from 2006 to 2018: SD, SC and SI (Figs. 3 and 5). Inclinometer measurements were carried out using a bi-axial Sinco Digitilt probe (Model 50310900 – S/N 42715) equipped with servo-inclinometer sensors (sensitivity 1/25000 senα). Data processing was performed using DigiPro2 software (Ver. 2.12.1.19169) by Slope Indicator Company. Fig. 5 shows ground deformation trends over time, highlighting both the total displacement (cumulative) and the changes between successive measurements (incremental) at each monitoring site, together with displacement over time at specific depths.

Cumulative displacement recorded by inclinometer SD over depth (upslope of Silvio North landslide, Fig. 5a) indicates that deformation is distributed across a broad interval, from approximately 0 to 21 m depth. Deformation was detected between approximately −11 m and −17 m depth. In the segment between −19 m and −21 m, displacement appears more localized, consistent with the presence of a deep-seated slip surface (Fig. 5b). At −20 m depth, a displacement of about 22 mm was recorded from near the beginning of the monitoring period, whereas the cumulative displacement over the −19 m to −21 m interval reached approximately 50 mm (Fig. 5a). The displacement trend between 19- and 21-m depth (along the +30° axis) indicates that the movement has continued at a nearly constant rate over time, suggesting a persistent but stable deformation along the slip surface (Fig. 5c). Notably, however, the inclinometer SD also shows signs of acceleration starting from the end of 2012, highlighting a possible change in the deformation dynamics.

Inclinometer SI (upslope of Silvio South landslide) has recorded, since the beginning of monitoring (2006), a deformation of approximately 6.75 mm at a depth of around 25 m (Fig. 5e). Additionally, in the depth interval between −23.5 and −28.0 m, cumulative displacement has reached approximately 40.5 mm, with a clear trend of decreasing displacement rate over time. This inclinometer is located at approximately the same elevation as SD, and indeed both show deep-seated slip surfaces. The displacement trend between 23.5 and 28.0 m (along the +10° axis) illustrates a clear temporal evolution (Fig. 5f): from 2012 to 2018, displacements

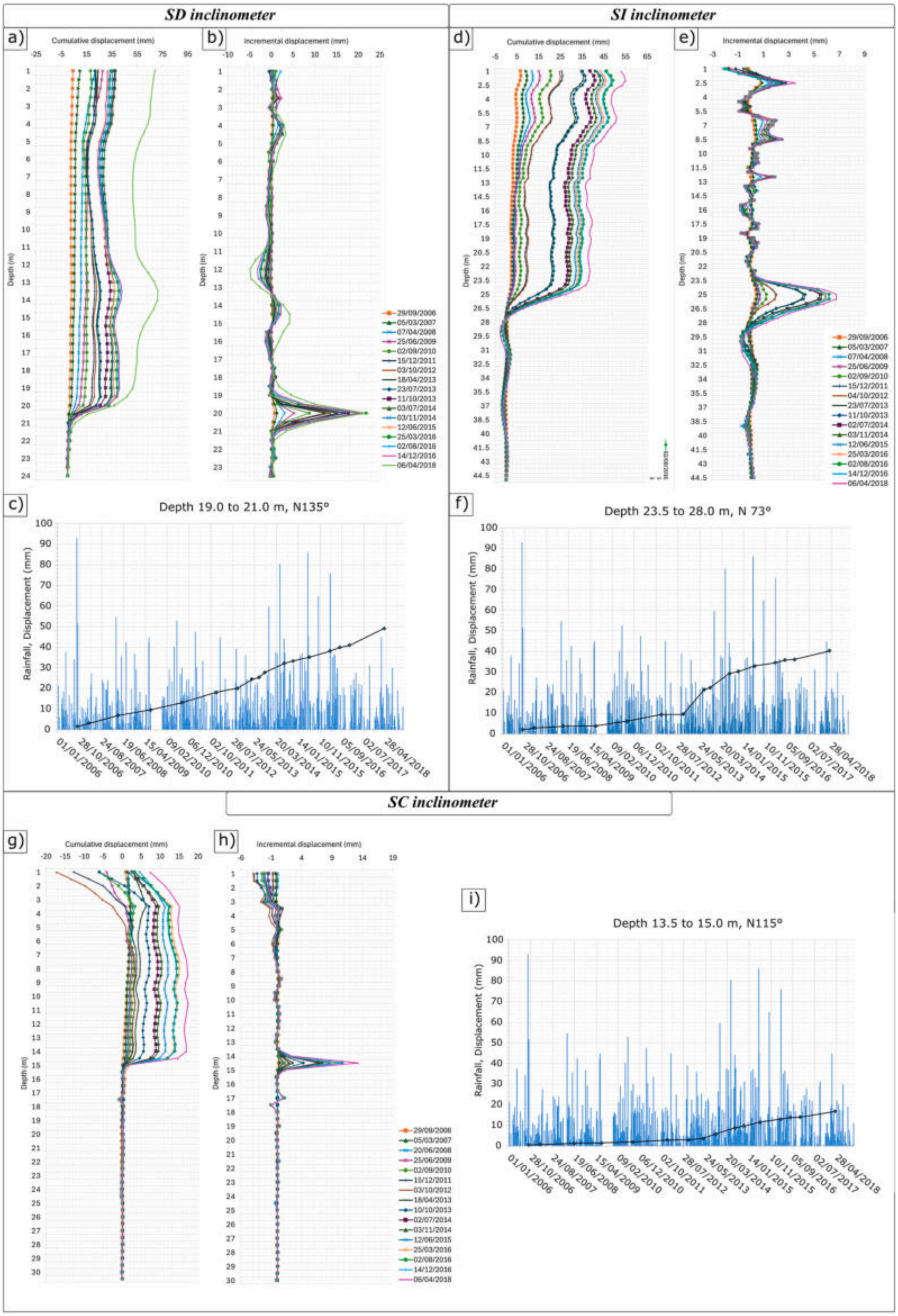

Fig. 5. Cumulative and incremental displacement profiles for inclinometers SD, SI, and SC: (a, d, g) cumulative displacements; (b, e, h) incremental displacements. Displacement trends over time at selected depths: (c) 19.0–21.0 m (SD); (f) 23.5–28.0 m (SI); (i) 13.5–15.0 m (SC). Inclinometer axis orientation is reported.

remained relatively low (below 10 mm), followed by a significant acceleration reaching 40 mm in 2018.

Inclinometer SC (footslope of Silvio South landslide) registers movement in the upper 15 m, with the maximum cumulative displacement (up to ∼18 mm) occurring between 3- and 15-m depth (Fig. 5g). The sharp transition in displacement suggests the presence of a shear zone or slip surface around 14–15 m depth (Fig. 5h), above which the landslide body is actively deforming. The displacement trend between 13.5 and 15.0 m (along the +5° axis) illustrates a clear temporal evolution (Fig. 5i): from 2006 to 2012, displacements remained relatively low (below 3 mm), followed by a significant acceleration starting in late 2012. By the end of 2017, cumulative displacement in this zone had reached approximately 17 mm, indicating a transition from a slow-moving to an active deformation phase, potentially linked to slope destabilization processes or external triggering factors, such as intense rainfall.

To further investigate the role of hydrological influence (e.g., rainfall vs groundwater dynamics), Fig. 6 presents the temporal evolution of the daily precipitation vs. piezometric levels measured in three different locations within the Silvio North and Silvio South landslide bodies, spanning from September 2006 to April 2018. The data correspond to piezometers SC', located at the footslope, and SD' and SI', situated in the upper part of the landslides. Over the monitoring period, SC' displayed a slight but consistent rise in the piezometric level, with a positive trend slope of $+8 \times 10^{-4}$ m/month, suggesting a gradual increase in water table elevation at the lower part of the slope. In contrast, both SD' and SI' showed decreasing trends in piezometric levels, with slopes of -1×10^{-3} m/month and -9×10^{-4} m/month, respectively. This indicates a gradual deepening of the water table in the upper parts of the landslide, with the same order of magnitude as the increasing level of the footslope (SC'). Only the years 2010–2012 are marked by a lowering in the piezometric level of SC' as a consequence of a prolonged hydrological dry period identified also by other authors in central Italy and even at the national scale [45,46]. The contrasting trends between the upper and lower piezometers reflect differential groundwater recharge, highlighting variable responses to external hydrological forcing (e.g., precipitation).

Indeed, the Extreme Rainfall Periodic Index (ERPI, [47]) is developed to assess the effect of hydrological drought and heavy rainfall events over the long term and the monitoring period. In particular, the sum of precipitation on days with extreme events (above the 95th percentile) is divided by the square of the sum of precipitation on days with rainfall exceeding 1 mm, thereby weighing extreme events in relation to the average rainfall on rainy days, this quantity is eventually multiplied by the long-term annual average precipitation following Eq. (1).

$$ERPI = \frac{\left(\sum_{1}^{m} P_d\right)_{>95^{th}}}{\left[\left(\sum_{1}^{m} P_d\right)_{>1mm}\right]^2} \, x \, \frac{\sum_{1}^{n} P_y}{n} \tag{1}$$

Where: P_d is the daily rainfall; P_y is the annual rainfall; m is the number of days; and n is the number of years.

The ERPI time series is analyzed over the period 1951–2018 (n = 68), through the Mann–Kendall test and Sen's Slope estimator (MAKESENS) technique [48] and it reveals a statistically significant increasing trend. The Mann-Kendall test yielded a standardized test statistic (Z) of 4.08 ($p < 0.001$), indicating a strong monotonic upward trend. The Sen's slope estimator further confirms this, with a median annual increase of 0.00265, and confidence intervals at both the 95 % and 99 % levels remaining entirely positive (Fig. 7). These results provide robust evidence of a non-random, positive trend in the ERPI index over the long term. Furthermore, the years 2006–2018 are marked by the higher ERPI values in its time series (0.86 in 2018, 0.87 in 2011, and 1.14 in 2009) suggesting that the altered rainfall dynamics, characterized by more extreme events, longer drought periods, and more intense storm rainfall, are limiting deep percolation and recharge toward the deeper layers and foster the recharge in shallower layers (Fig. 6). The decline in the piezometric level recorded in SC' between 2010 and 2012 is also strongly associated with the decrease in ERPI values during the same period (except in 2011), a result that aligns with the dry conditions reported by other authors [49].

This effect is likely due to the reduced thickness of the unsaturated zone in the footslope area, which results in a shallower water table. This is consistent with the observed deposit thicknesses of 13.1 m and 11.4 m in sites SD' and SI', respectively, compared to only

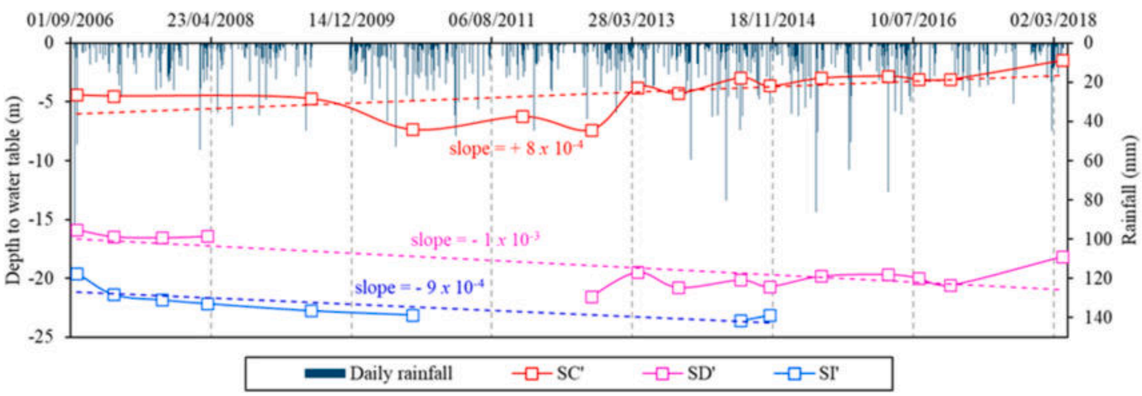

Fig. 6. Daily rainfall and piezometric levels monitored in SD', SI' (upper slope) and SC' (footslope), with linear trend (dashed lines) and its angular coe between September 2006 and March 2018.

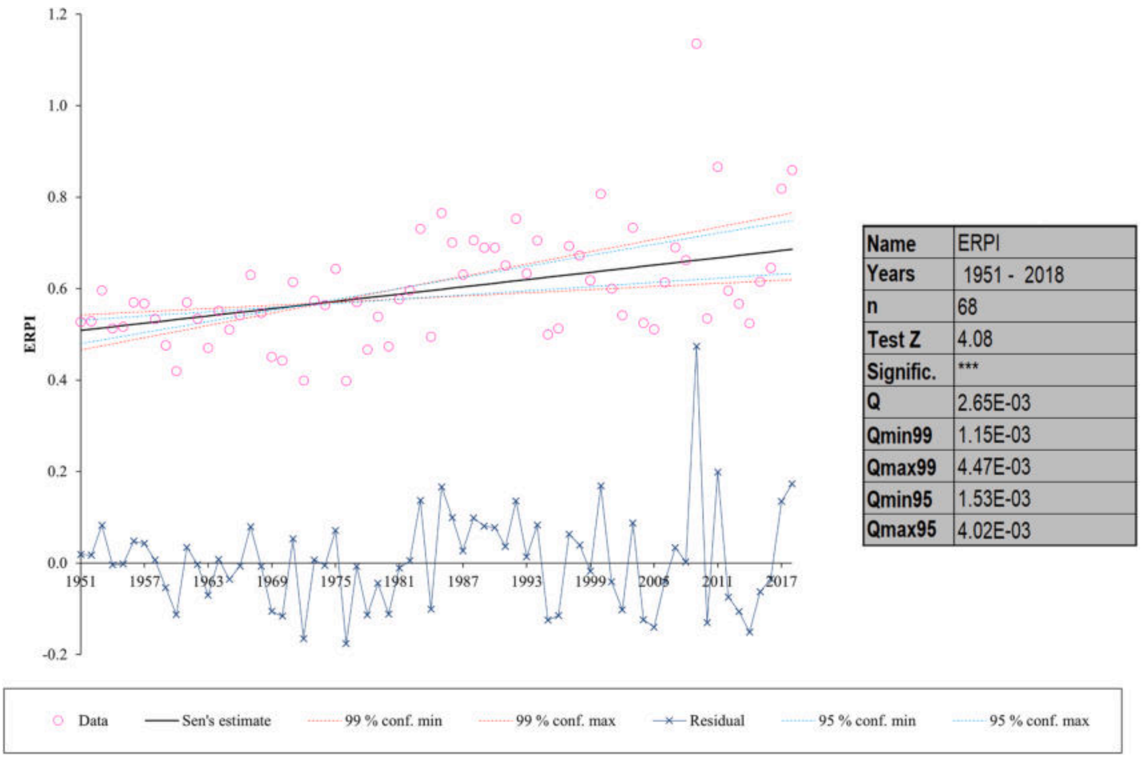

Fig. 7. Extreme rainfall and periodic index (ERPI) tested from 1951 to 2018 with the Mann–Kendall test and Sen's Slope estimator, displaying confidence values for 95th, 99th percentiles and residuals.

5.5 m in site SC'. These findings align with groundwater patterns documented by Fronzi et al., [50,51] on the western oriented slope of Monte Conero. Consequently, a shift in hydraulic pressure from the upper to the lower slope is observed and single storm rainfall may contribute more significantly to recharge with a short-term effect in the fooslope. In brief, while the upper slope of the landslide area shows a depletion of the groundwater level due to increased drought periods alternating with intense rainfall events, the footslope exhibits a rising groundwater table. This rise is likely driven by the temporal distribution and intensity of rainfall, with visible effects confirmed by trench observations in the lower slope.

4.2. DInSAR data

The back-monitoring of the ground movements in the study area has been performed by analysing Differential Interferometric Synthetic Aperture Radar (DInSAR) data. This technique is a well-known and widely used method for detecting and monitoring slow-moving landslides [52,53]. Specifically, COSMO-SkyMed and Sentinel-1 data were used. The COSMO-SkyMed (CSK) data are provided by the Italian Ministry for the Environment, Territory and Sea by means of the national geoportal (Geoportale Nazionale—GN) and the CSK SAR images cover the period 2011–2014 including ascending (asc.) and descending (desc.) order of geometry and high-resolution X-band data [54]. The CSK SAR images were processed using the PSInSAR™ [55] and PSP-DifSAR approaches [56]. The Sentinel-1 data are provided by the Copernicus European Ground Motion Service (EGMS) [57] and we used the first release of mid-2024, which offers ground displacement data for the period 2018–2022 with sensors in C-bands. This service allows to download three main products named as Basic, Calibrated and Ortho. The Basic products correspond to line-of-sight (LOS) deformation velocity and time series for each measurement point (MP). The Calibrated products are obtained starting from the Basic products and using a referenced to a deformation velocity model derived from GNSS data. Movements away from and toward the sensor mounted on the satellite's board and the measurement point are indicated by negative and positive values, respectively. The Ortho products provide vertical and east-west (horizontal) displacements in 100 m × 100 m output resolution cells [58]. It is worth noting that the ERS1/2 and ENVISAT datasets from the Not-Ordinary Plan of Environmental Remote Sensing (Piano Straordinario di Telerilevamento Ambientale, PST-A) were also examined to assess ground movements for the periods 1992–2000 and 2003–2010, respectively. However, the measurement point density was insufficient to analyze earlier movements. Indeed, the study area includes several landslides characterised by the widespread presence of vegetation, that causes temporal decorrelation, affecting the identification of stable measuring points [59]. As shown in Fig. 8, CSK and Sentinel-1 ascending and descending measuring points are detected in the Silvio North landslide, specifically in proximity of a local urbanized area, where inclinometer (SD) and piezometers (SD') are available. However, the available data are available only for the period of the CSK data. In the period 2011–2014, this urbanized area records average LOS velocity of −11.03 ± 0.44 mm/yr and 5.8 ± 0.04 mm/yr, using CSK asc.and desc., respectively. In the period 2018–2022, the

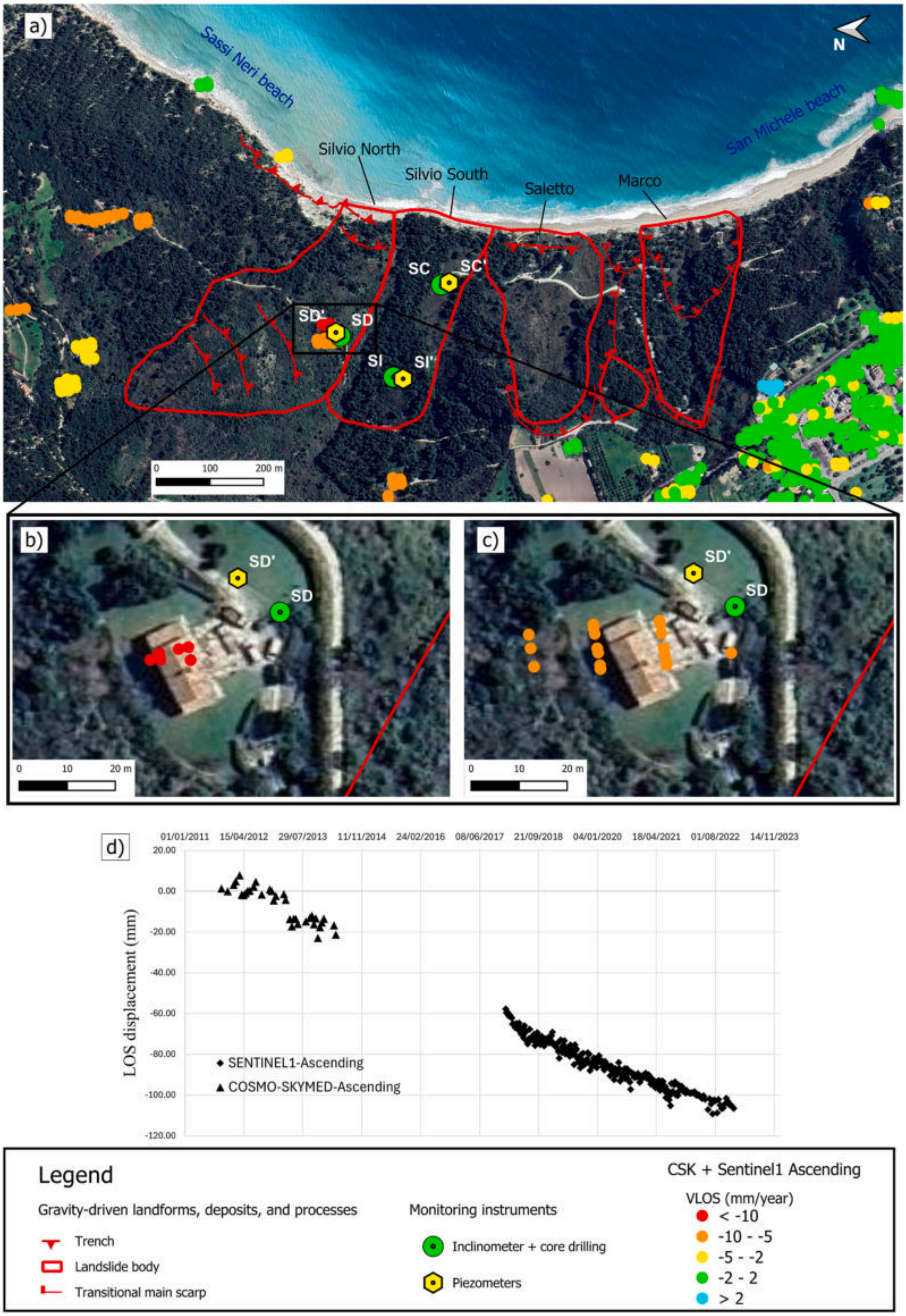

Fig. 8. Distribution of ascending DInSAR measuring points from EGMS Sentinel-1 data in the study area (a). Figures (b) and (c) provide a zoom of the average LOS velocity rate measured using the COSMO-SkyMed and Sentinel-1 InSAR asc. datasets near the inclinometers and piezometers for the periods 2011–2014 and 2018–2022, respectively. (d) LOS displacement time series of the measuring points located in the Silvio North landslides.

measured average LOS velocity is −9.20 ± 2.03 mm/yr and 3.13 ± 0.9 mm/yr, using Sentinel-1 asc.and desc. datasets. Considering the aspect of the slope (south-east-facing), this landslide can be better investigated using DInSAR data acquired in ascending geometry. Considering the CSK and Sentinel-1 datasets, all measurement points showed a LOS velocity higher than −2 mm/y for both acquisition periods of these satellites, confirming that the landslide was active during the monitored periods as observed using the SD inclinometer measurements. The average cumulated displacements reach values of 20.81 ± 1.38 mm and 48.36 ± 9.24 mm in the period 2011–2014 and 2018–2022, respectively. The EGMS ortho products gives insight about −4 mm/yr and 8 mm/yr for the vertical and east-west components. Therefore, the urbanized area in the Silvio North landslide shows higher values of the movements toward east. The displacement time series show linear trend of the ground deformation for the period 2011–2024, whereas non-linear trend is detected for the period 2018–2022.

4.3. Historical evidence of footslope processes

Toppling and collapse phenomena affecting the colluvial/landslide deposits of the Scaglia Cinerea Fm., extensively exposed along the coastal cliff (Fig. 4), have occurred repeatedly over recent decades, both with minor and major collapses. These footslope processes are not currently monitored by dedicated instrumentation. Nevertheless, the occurrence of major collapse events has been documented through firsthand accounts from local residents, providing valuable qualitative evidence of slope activity.

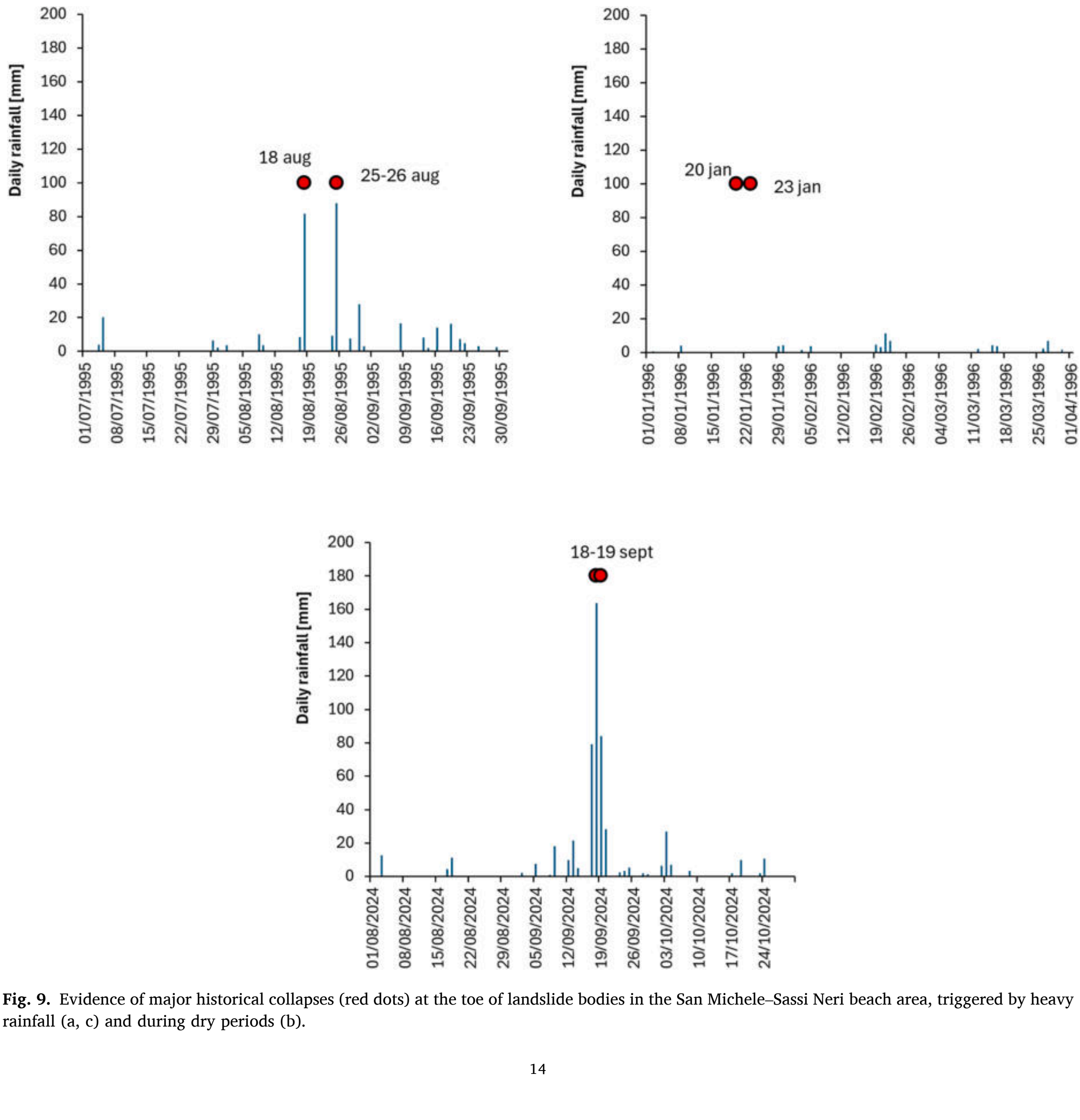

Fig. 9. Evidence of major historical collapses (red dots) at the toe of landslide bodies in the San Michele–Sassi Neri beach area, triggered by heavy rainfall (a, c) and during dry periods (b).

Fig. 9 presents four recorded collapse events that took place between 1995 and 2024, alongside daily rainfall data. A clear temporal correlation is observed between some collapses and high-intensity rainfall. Specifically, the events of 18 August and 25–26 August 1995 occurred along with daily precipitation of 80 mm and 90 mm, respectively. Similarly, the collapse episodes of 18–19 September 2024 were triggered during an extreme rainfall event, which registered 164 mm in 24 h, leading to two significant failures along the shoreline. Conversely, the collapses recorded on 20 and January 23, 1996 were not preceded by substantial rainfall, suggesting that precipitation is not the sole triggering factor. It is highly likely that numerous smaller-scale collapse events have occurred over the years along the coastal slope. However, due to the absence of direct observations or documented eyewitness accounts, these minor failures have gone unrecorded. The collapses considered in this study are all events that directly impacted the beach, depositing debris that were subsequently reworked and redistributed by wave action and coastal erosion. These processes highlight the dynamic and evolving nature of the slope-beach system, where debris failure can be rapidly removed by marine processes, effectively erasing the geomorphic evidence of recent collapses. This underscores the need to implement a dedicated monitoring system for the coastal sector, aimed at systematically recording the frequency, magnitude, and spatial distribution of both major and minor failure events. Establishing such a monitoring framework would not only improve hazard assessment but also enable a more detailed understanding of the triggering mechanisms, including but not limited to rainfall. Monitoring would allow for the investigation of additional controls such as rock mass fatigue, progressive fracturing, coastal toe erosion, and hydromechanical weakening, which may act in concert with or independently from meteorological forcing.

5. Exposure drivers and seasonal tourism

The exposure of coastal areas to tourism-related pressures strongly depends on the seasonal variation of occupancy rates. To better understand and quantify this aspect, remote sensing data can be used to estimate the distribution and intensity of tourist presence over time. In this framework, object detection is a common task in computer vision that involves identifying and localizing objects within an image through bounding boxes. YOLO (You Only Look Once) is a state-of-the-art object detection approach with a good balance between speed and accuracy. YOLO v11 [60] represents an evolution over previous versions. Unlike traditional approaches that use a two-stage detection pipeline, YOLO v11 performs object classification and bounding box regression in a single forward pass, making it highly efficient for large-scale image analysis.

To enhance the model's generalization capabilities and reduce overfitting, we employed different data augmentation techniques. We considered flip (both vertical and horizontal) and rotation ($\pm 15^\circ$) and hue/saturation/value.

To build our dataset, we collected a series of high-resolution images of the area of interest using Google Earth. We started to analyze the available dates for the area of interest. Over 11 potential dates (from 2012 to 2024) only 5 have been used due to acquisition dates (we excluded winter, autumn, and early spring). Each image has been georeferenced and co-registered using QGIS Desktop 3.40.4 using a wide set of target points to ensure a proper overlap between the images. Points have been selected in areas that are not subject to erosion/sea currents. The typical GSD of derived images was in the range 0.2–0.3m. The analysis was restricted to an area of 9ha (Fig. 10a).

The annotation process was designed to identify five different classes.

- Parasol [feasible to detect]

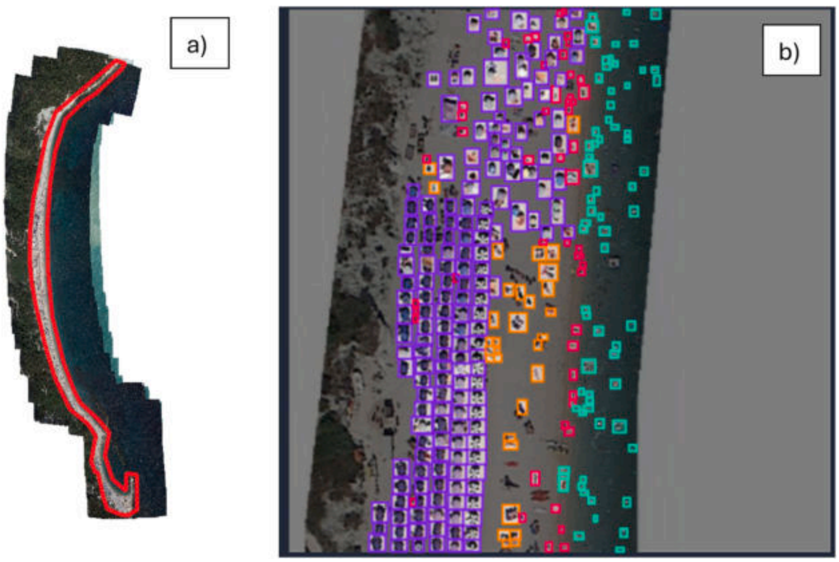

Fig. 10. Orthophoto of study area with a red polygon that represents the study area (a), and example of tile with different annotated classes (b); the available classes are purple: parasol; green: person in water; red: person; orange: sunbed.

- People-parasols [complex class due to image resolution and lack of details]
- Person [complex class due to image resolution and lack of details]
- Person in water [complex class due to image resolution and lack of details]
- Sunbed [complex class due to image resolution and lack of details]

We decided to annotate all these classes even if after first training of YOLO v11 model we discovered that classes as Sunbed, Person and Person in water achieved poor results. This is mainly attributable to poor resolution of the images. Even if the GSD was around 0.3m, the quality was poor due to limitations of images derived from the web version of Google Earth. Before starting the training phase for each image, we decided to derive tiles (smaller size) to avoid issues during the inference phase. We selected 70 % of the images for training, 20 % for validation, and 10 % for testing. Fig. 10b shows an example of an annotated tile; a tile is an image of 512x512px that represents a small portion of the study area. We used 200 epochs for training. On date 20130804 (Sunday) we detected 1550 parasols; on 20160522 (Sunday) 248 parasols; on 20170831 (Thursday) 1350 parasols; on 20210622 (Tuesday) 1046 parasols and on 20230705 (Wednesday) 1026 parasols. The average precision by class (mAP50) for parasols was 77 %. From the analysis of collected images, we discovered that some images are characterized by poor quality (high distortion) impacting detection performance. It is also important to consider that for the same area the parasols could have different configurations over time depending on the day of the week (during the middle of the week some parasols are closed) also impacting the final counting. If we consider the date with the highest number of opened detected parasols, we can try to estimate the number of people. During the full season if we consider 1 to 3 people/parasol this implies a maximum number of 4950 people. This estimation does not consider of course people on sunbed without a parasol that are usually present. The detection accuracy could be improved with more samples using higher quality images. The use of Google Earth image cannot ensure the same results of using high quality remotely sensed images (e.g. Pléiades) that will be evaluated in future works.

Two limitations apply to the data underpinning this approach. First, the estimation of tourist attendance could not be continuously validated against independent in-situ counts; as a result, the temporal fidelity of the exposure signal is partial and would benefit from systematic ground-based monitoring. Second, the YOLO-based detection was trained on a relatively small dataset constrained by the availability and resolution of Google Earth imagery, which limits model robustness and generalizability and indicates the need for larger and more diverse datasets in future applications. Acknowledging these limitations, we interpret exposure values conservatively. Nonetheless, the method offers the only reproducible, spatially explicit proxy of beach occupancy currently available for this site and thus a defensible basis for the risk analyses presented here.

6. Tourist awareness of landslide risk

6.1. Analyzing risk perception in a high exposure setting

According to their setting and their accessibility, San Michele and Sassi Neri are the signature “wild beaches” of the Sirolo coastline. We showed that on a peak summer day, the deep learning model counts of parasols and bathers peak to around 4950 people spread over just 22000 m2 of shoreline, a density of almost 0.225 beachgoers per square meter. As mentioned, in 2023, while Sirolo had a resident population of 4098 inhabitants, the town attracted a total of 55368 tourist visitors [61]. Consequently, summer tourism represents a significant factor, influencing both the local economy and the risk dynamics. Indeed, whereas local residents might be aware that minor rockfalls are recurrent and that major collapses (e.g., the 1962 “Frana del Saletto”) can reach the swash zone and even determine the shoreline advancement [44], the vast majority of beach users are day-trippers or holidaymakers. Most of these visitors, who typically arrive via shuttle bus, hiking trails, or by boat, do not reside in Sirolo and therefore they might lack routine

Table 2
Content of the structured interviews administered to Sirolo tourists.

#	Question	Response options	Rationale
1	Gender	F/M/Other	Gendered differences in risk perception.
2	Age	<30, 30–40, 40–50, 50–60, >60	Life-experience effect.
3	Place of residence	Open	Resident vs non-resident.
4	“Floods are an exceptional event in Sirolo”	Likert scale: 1 (strongly disagree) - 5 (strongly agree)	Mask the landslide topic.
5	“Landslides are an exceptional event in Sirolo”	Likert scale: 1 (strongly disagree) - 5 (strongly agree)	Core perception variable.
6	“Earthquakes are an exceptional event in Sirolo”	Likert scale: 1 (strongly disagree) - 5 (strongly agree)	Mask the landslide topic + explore coastal seismic risk perception.
7	Most frequently visited beach in Sirolo	Open	Targeting of communication.
8	“Trails to the beaches are easily walkable”	Likert scale: 1 (strongly disagree) - 5 (strongly agree)	Access constraints, evacuation feasibility.
9	Mobility impairments (self/acquaintances)	Yes/No	Differential vulnerability.
10	Previous involvement in a natural-hazard event	Open	Salience of past hazard experience.
11	Knowledge of the Sirolo civil protection plan	Yes/No	Preparedness indicator

familiarity with local slope conditions, hazard signs, and evacuation procedures. Paradoxically, the very features that make the beach attractive (seclusion, high cliffs, and remote access) also increase the vulnerability of these non-resident visitors in the event of a landslide. Their limited local knowledge, coupled with the narrow, funnel-shaped trails and the scarcity of escape routes, makes them particularly susceptible to risk during such events.

To better understand this vulnerability, we administered an 11-item face-to-face interview (Table 2) to non-resident visitors along beach access trails and shorelines, within the period July–September 2023. To limit selection and clustering biases, respondents were intercepted through systematic random sampling along pre-defined beach access trails and shoreline segments, proceeding at fixed spatial intervals and with at most one respondent per group until the target was reached. According to the Cochran formula for estimating sample size, adjusted for finite populations [62], considering the most conservative variance assumption (p = 0.550), a 90 % confidence level, a 10 % margin of error and a population of 55.000 summer visitors, it is required a minimum sample of 67.57 respondents (approximated to 68). The structured interviews were conducted in Italian, with a completion time of average 6 min, to ensure full comprehension of technical terms and to avoid language-related measurement bias and the responses were coded immediately on a tablet via an anonymized form. Responses were coded immediately on a tablet, anonymized and exported to a spreadsheet for descriptive statistics.

The interview followed a deductive structure that eased respondents from simple facts into increasingly focused reflections. It opened with a brief demographic investigation (questions 1–3) that asked only for gender, age and place of residence to sketch the sample profile without causing fatigue to the respondent. The second block (questions 4–7), shifted to perceptions and situational awareness. Three 5-point Likert statements (from 1 strongly disagree to 5 strongly agree) analyzed how exceptional respondents judged floods, landslides, and earthquakes to be in the Municipality of Sirolo, while an open question identified the beach they frequented most. Placing the landslide item beside two equally plausible hazards diluted any cue that it was the “real” topic, helping to curb priming bias. Finally, the survey deepened into practical vulnerability and preparedness (questions 8–11). A Likert item on trail walkability measured perceived ease of evacuation; a yes/no question captured any mobility impairments in the party; an open item recorded past experience with natural hazards; and a closing yes/no query probed awareness of Sirolo civil-protection plan. By progressing from straightforward facts through attitudinal judgments to concrete readiness, the survey kept respondents engaged while systematically reducing response bias.

The face-to-face survey captured 68 respondents. From a methodological perspective, the 68 completed interviews meet Cochran’s criteria for estimating simple proportions at the selected confidence level. However, the dataset remains too limited for reliable multivariate modeling, so we report only descriptive results with confidence intervals that are corrected for the finite population. A larger follow-up survey, ideally with a doubled sample size, would enable interaction testing with sufficient statistical power. That said, it is important to acknowledge the inherent challenges of surveying tourists, who are often difficult to engage in due to their relaxed, holiday-oriented mindset. Temporal coverage also warrants caution. Fieldwork took place in mid-summer, between late morning and late afternoon; early hikers and sunset bathers were missed, and their awareness profiles might diverge. Lastly, the face-to-face setting, while excellent for response rates, may have encouraged socially moderate answers. An anonymous, QR-code self-administered version could test for social-desirability bias and reach tech-savvy visitors who avoid interviews.

From a demographic point of view, respondents of the interview were predominantly female, accounting for 56 % of the sample, compared to 41 % male respondents. An additional 3 % identified as non-binary or preferred not to specify their gender, reflecting a modest but notable diversity in gender representation (Table 3a). Although females slightly outnumbered males, this difference is not substantial enough to suggest a significant bias in the overall sample. Regarding age distribution, respondents demonstrated a marked skew toward younger visitors. Specifically, the largest age group consisted of participants younger than 30 years old, representing 35 % of the sample, followed by nearly equal proportions in the 30–40 (23 %) and 40–50 (26 %) age brackets. A smaller share of participants was found in the 50–60 age range (12 %), while respondents older than 60 constituted just 4 % of the sample, highlighting the predominance of a younger tourist demographic. Moreover, interviewees originated from fifteen Italian regions, ensuring strong geographical heterogeneity within the sample. Within the Marche region itself, the province of Ancona was the most represented, with 18 respondents. Additionally, visitors from Tuscany, Lombardy, and Emilia-Romagna were particularly numerous, with Tuscany emerging as the single most represented region outside Marche. Nevertheless, the overall sample effectively mirrored the diverse geographical composition characteristic of Sirolo summer visitors.

Perceptions of hazard frequency revealed a substantial awareness gap among respondents (Table 3b). Remarkably, despite being interviewed directly in a cliffside environment beneath the clearly visible slopes of Monte Conero, respondents expressed considerable uncertainty regarding the rarity of landslides. Confronted with the key statement “Landslides are an exceptional event in Sirolo”, more than half (51 %) disagreed, implicitly suggesting their perception that landslides might not be rare occurrences in the area. However, a substantial portion of respondents (35 %) selected a neutral position, indicating either hesitation, uncertainty, or a lack of confidence in their own knowledge. Only a minority (13 %) clearly agreed with the statement, explicitly perceiving landslides as rare phenomena. This pattern suggests that, while respondents do not fully reject the possibility of frequent landslides, they also encounter difficulty in clearly identifying their frequency, potentially due to a lack of direct experience, limited information, or the deceptive tranquility presented by the scenic coastal landscape. Notably, the surveyed individuals predominantly consisted of habitual visitors to the study-area beaches of Sassi Neri and San Michele (38 % and 32 %, respectively). Thus, their uncertainty regarding landslide frequency appears even more significant, given their prior familiarity with the local beaches and presumably higher awareness of the surrounding environment. The inclusion of additional masking items (regarding floods and earthquakes) helped contextualize these results (Fig. 11). Responses to the statement "Floods are an exceptional event" displayed a different pattern, characterized by stronger disagreement: 41 % of respondents partly disagreed, while the share of uncertain respondents was lower (24 %). This likely reflects the familiarity with heavy-rain events within the Marche region. Conversely, perceptions regarding earthquakes yielded more evenly

Table 3
Distribution of survey responses from tourists in Sirolo, presented as absolute frequencies (Total N = 68) and percentages (%) of the actual respondents. Table 3a reports demographic characteristics, Table 3b perceptions and situational awareness, Table 3c vulnerability and preparedness.

Response category	N	%
1 – Gender		
Female	38	55.9
Male	28	41.2
Other/No answer	2	2.9
2 – Age class		
<30	23	34.3
30–40	16	23.9
40–50	17	25.4
50–60	8	11.9
>60	3	4.5
3 – Place of residence (by region)		
Marche (Ancona province)	18	27.3
Tuscany	7	10.6
Marche (other provinces)	6	9.1
Lombardy	6	9.1
Emilia-Romagna	5	7.6
Puglia	4	6.1
Abruzzo	3	4.5
Lazio	3	4.5
Liguria	3	4.5
Sicily	2	2.2
Piedmont	2	2.2
Veneto	2	2.2
Trentino Alto Adige	2	2.2
Other IT regions	3	4.5

Response category	**N**	**%**
4 – "Floods are an exceptional event"		
1 – Strongly disagree	6	8.8
2 – Partly disagree	28	41.2
3 – Uncertain	16	23.5
4 – Partly agree	6	8.8
5 – Strongly agree	12	17.6
5 – "Landslides are an exceptional event"		
1 – Strongly disagree	13	19.1
2 – Partly disagree	22	32.4
3 – Uncertain	24	35.3
4 – Partly agree	2	2.9
5 – Strongly agree	7	10.3
6 – "Earthquakes are an exceptional event"		
1 – Strongly disagree	14	20.6
2 – Partly disagree	13	19.1
3 – Uncertain	18	26.5
4 – Partly agree	8	11.8
5 – Strongly agree	15	22.1
7 – Most frequently visited beach		
Sassi Neri	26	38.2
San Michele	22	32.4
Urbani	16	23.5
Le Due Sorelle/other	4	5.9

c)	Response category	N	%
VULNERABILITY AND PREPAREDNESS	**8 – "Trails are easily walkable"**		
	1 – Strongly disagree	3	4.5
	2 – Partly disagree	13	19.4
	3 – Uncertain	23	34.3
	4 – Partly agree	8	11.9
	5 – Strongly agree	20	29.9
	9 – Mobility impairments		
	Yes	9	13.4
	No	58	86.6
	10 – Previous natural-hazard experience		
	Yes, earthquake	12	17.6
	Yes, flood	3	4.4
	Yes, severe storm/hail	3	4.4
	No/No answer	50	73.6
	11 – Knowledge of civil-protection plan		

(*continued on next page*)

Table 3 (*continued*)

	Yes	1	1.5
	No	67	98.5

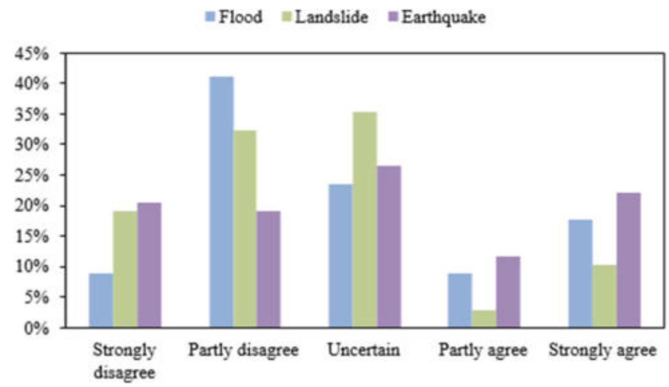

Fig. 11. Comparison of responses concerning perception and awareness of flood (blue), landslide (green), and earthquake (purple) hazards, based on interviewees answers to questions 4–6. The original Likert-scale statement was: "Floods/landslides/earthquakes are exceptional events in the Municipality of Sirolo".

divided responses, with 40 % disagreeing that earthquakes are exceptional, 34 % agreeing, and 26 % remaining uncertain. Such a balanced distribution indicates a moderate awareness of the actual regional seismic hazard.

For what concern the vulnerability of the respondents, opinions regarding accessibility and trail conditions were notably mixed (Table 3c). While nearly half of the participants (42 %) agreed that the trails were easily walkable, a considerable proportion (34 %) indicated uncertainty, choosing a neutral position. Additionally, nearly a quarter of the respondents explicitly disagreed (24 %), highlighting perceived challenges regarding the use of trials. In this context, it is notable that 13 % of respondents reported the presence of mobility impairments, either personal or involving someone within their group, further emphasizing accessibility concerns. Finally, preparedness levels among respondents emerged as alarmingly low. Virtually all respondents (99 %) indicated they were unaware of the local municipal civil protection plan, with only one person demonstrating knowledge of established emergency procedures. Furthermore, when considering previous natural-hazard experiences, about one-fourth of respondents (26 %) reported exposure to past hazardous events. Earthquakes were the most frequently mentioned (18 %), followed by floods and severe meteorological events such as hailstorms, each cited by 4 % of participants. Significantly, the majority (74 %) either had no such experience or did not respond. This low direct hazard experience, coupled with extremely limited awareness of the local emergency management procedures, indicates substantial vulnerability within this visitor population, despite their familiarity with the beaches themselves.

6.2. *Interpreting the perception-exposure mismatch as a vulnerability*

The results portray a picture of high physical exposure set against modest preparedness. Although thousands of people crowd the toe of an active cliff each summer day, 13 % of them believe landslides are "exceptional", while one third remain unsure. In practical terms, approximately half of the beach users either underestimate or cannot adequately gauge the likelihood of slope collapse, revealing both an information deficit and a classic optimistic bias, that is the common tendency among individuals to downplay risks, especially in recreational or holiday settings [63].

This gap can be better understood in light of psychological theories of risk perception. In fact, risk perception is not purely rational but involves physical, cognitive, and emotional components [16]. In the context of tourism and leisure, voluntary exposure and perceived control over one's activities and surroundings can lead individuals to underestimate objective threats, perceiving hazards as less relevant or less likely to occur [64]. Slovic [16] posits that two main factors interactively shape public perceptions of risk: knowledge, that is familiarity and understanding of the hazard, and dread, namely the perceived severity of potential consequences. When a hazard is poorly understood but evokes fear, perception tends to be heightened. Conversely, in scenarios such as the Sirolo beaches, where landslides evoke low dread (due to the lack of direct experience) and are poorly understood by non-resident visitors, perceptions of risk tend to be notably lower. This is consistent with the observed uncertainty in respondents' answers. Moreover, Bubeck et al. [15] highlight the critical role of personal experience with disasters in shaping accurate risk perception. The observed lack of any local landslide experience among interviewees significantly weakens their hazard awareness and diminishes preparedness efforts. The absence of memory, familiarity, or direct encounters with slope instability thus contributes substantially to their vulnerability.

The mismatch is further amplified by the non-resident composition of the tourist population. Most visitors, residing outside the municipality and region, have not developed familiarity with visual cues indicative of slope instability, such as surface cracks, displaced boulders, or vegetative shifts, which local residents might notice and interpret as signs of impending risk. Consequently, even if hazard warnings or signage are present, visitors might overlook, misunderstand, or disregard them, perceiving such indicators as irrelevant or non-threatening elements of the natural landscape rather than urgent safety communications.

Furthermore, the substantial knowledge gap regarding municipal emergency plans greatly exacerbates this situation. With 99 % of respondents reporting no awareness of the local civil protection plan, evacuation strategies in a critical scenario would depend heavily on immediate external intervention by lifeguards, local authorities, or emergency alerts delivered digitally, rather than on prior individual knowledge or self-organization.

Eventually, the observed behavioral data highlight practical constraints. With approximately one-quarter of respondents perceiving the access trails as difficult to traverse, and an additional one-third uncertain about trail conditions, a sizable fraction of

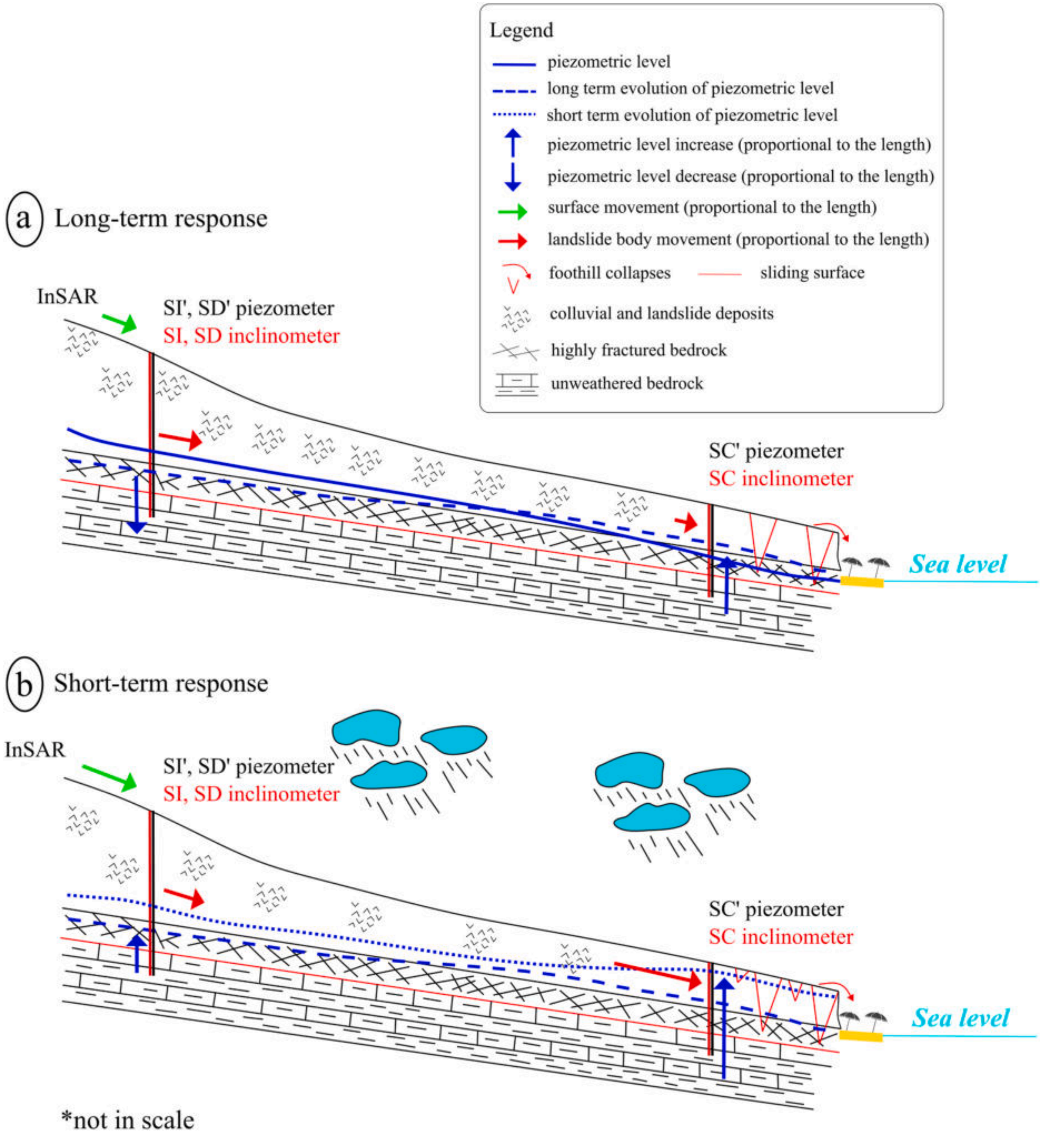

Fig. 12. Conceptual model of landslide kinematic and hydrogeological conditions under long-term (a) and short-term (b) response to external triggering factors (i.e., precipitation).

beach users might hesitate or experience difficulty during emergency evacuations. Such hesitation could critically slow down evacuation processes, heightening exposure and potential injury.

In summary, the identified perception–exposure mismatch constitutes a significant vulnerability. Tourists are physically exposed yet mentally unprepared or insufficiently aware of the risks associated with landslides. Addressing this critical gap through improved information dissemination, clear visual and textual warnings, and structured preparedness training is fundamental to strengthening community resilience and developing robust, effective Disaster Risk Reduction strategies for coastal tourism areas.

7. Discussion

7.1. Landslide mechanisms

The integration of hydrological and inclinometric monitoring (Fig. 5) enables the identification of two distinct triggering mechanisms of slope instability in the area, making it a singular case from a landslide hazard perspective. The first mechanism (Fig. 12a) is associated with prolonged drought periods, which results in limited recharge of the groundwater body of the landslide. This lack of recharge leads to a lowering of the piezometric level in the upslope sector and causes shrinkage of the clay matrix, leading to increased fracturing and higher permeability in the weathered bedrock (Table 1), as evidenced by Li et al. [65]. This long-term process induces a progressive decreasing trend in the piezometric levels observed in the upslope piezometers (SI' and SD'), causing a gradual transfer of hydraulic pressures downslope (SC') (Figs. 6 and 12a).

As a result, the upper slope sector of the landslide is subjected to permanent movements higher than −2 mm/yr, with a main translational horizontal component towards the sea, as supported by the opposite signs of the ground movements detected by the two satellite DInSAR acquisition geometries (i.e. asc. and desc.) and confirmed by the inclinometric measurements. The long-term effect tends to increase pore pressure at the landslide toe even during dry periods. The second mechanism is related to the short-term triggering caused by intense rainfall (Fig. 12b), enhancing slope instability at the footslope of the landslide.

Indeed, individual extreme rainfall events or precipitation events occurring during particularly wet periods induce a response in the groundwater system, especially where the piezometric level is shallower (SC', at the toe of the landslide, Figs. 6 and 12b), due to thinner colluvial/landslide deposits (Table 1 and Fig. 12). These events are linked to faster slope movements, such as those recorded between October 2012 and March 2013 (Fig. 5), which initiated at the landslide toe (Fig. 5g, h, i) and propagated upslope (inclinometer SI, Fig. 5d, e, f). In fact, the groundwater body is inferiorly confined by the unweathered bedrock of Scaglia Cinerea Fm. and involves the fractured bedrock and the colluvial/landslide deposits, as shown by piezometric data and stratigraphic correlations (Table 1).

Under the effect of the two identified hydrogeological conditions, the main sliding surface involves the interface between the unweathered bedrock and its fractured portion (Fig. 12), where groundwater pore pressure is concentrated. During drought periods, the migration of groundwater from the upslope to the footslope sector of the landslide leads to movement of the landslide body along the sliding surface. This process causes progressive compaction and subsidence in the upslope sector, while promoting groundwater flow downslope. The increased water pressure at the landslide toe, where the beach is located, generates a thrust that often results in collapses and slope failures. Conversely, during intense rainfall events, the rapid and more pronounced rise in groundwater levels in the footslope sector triggers more evident and rapid collapses. This is due to the sudden increase in pore water pressure and the consequent destabilization of the landslide toe. Therefore, the footslope processes involving the beach can occur both following intense rainfall events (Fig. 9a–c) and during particularly dry periods (Fig. 9b).

For the sake of scientific clarity, it is important to acknowledge that piezometric monitoring in the study area is discrete rather than continuous, as is commonly the case in long-term hydrogeological investigations of landslides. This limitation prevented us from establishing a formal statistical correlation between rainfall, piezometric fluctuations and landslide displacements/collapse. Nevertheless, we evaluated the relationship between rainfall patterns (through the ERPI, tested for monotonic trends) and the observed increases or decreases in groundwater levels during the available measurement campaigns. As a result, the link between rainfall and slope kinematics should be regarded as an empirical correlation rather than a statistically validated causal relationship. This constraint emphasizes the need for future continuous hydrogeological monitoring to enhance improve the reliability of rainfall–landslide interaction models.

Marine erosion represents an additional conditioning factor in the evolution of the slope [66]. However, it should be noted that on the studied sector this process becomes effective only during particularly stormy days, when intense wave motion allows seawater to reach the foot of the landslide, which is otherwise protected by the presence of the beach. In such conditions, the presence of visitors on the beach would be negligible or absent, implying that the immediate risk to people would be close to zero. Nevertheless, it is advisable to integrate monitoring at the landslide toe in order to evaluate possible overpressures generated by storm-wave impacts, which could in turn lead to delayed slope movements or collapses, even several days after the triggering event. However, at present, this dataset is not available to the authors and although it could represent a field to be deepened in the future, it is beyond the purpose of this study.

Finally, the Conero area has been affected by significant seismic events, the most recent of which occurred on November 9, 2022 (magnitude ~5.5; e.g., Refs. [41,67–69]). These earthquakes induced rockfalls mainly in the highest and steepest rocky sectors of the promontory [67,70] where topographic amplification effects were relevant. Conversely, the landslides investigated in this work develop on colluvial and landslide deposits with relatively low slope angles, where seismic shaking has not been observed to directly trigger failures. For this reason, although seismicity is an important regional trigger, its influence on the studied landslides is considered to be limited.

7.2. Proposed landslide risk mitigation strategies

The Sirolo coastal system presents a unique case of landslide risk that calls for hybrid and site-specific mitigation strategies, tailored to its physical fragility, environmental value, and intense seasonal use. As shown, slope instability results from two complementary processes, long-term stress redistribution during dry periods and short-term triggering from intense rainfall. Therefore, the risk cannot be addressed through a singular lens. Rather, it requires the integration of geomorphological diagnostics, adaptive structural interventions, targeted communication, and community involvement.

From a structural perspective, the environmental and landscape constraints of the Monte Conero Regional Park necessitate low-impact, nature-based solutions. For instance, slope re-profiling using wooden containment systems (e.g., double-wall palisades) built from durable chestnut timber could stabilize selected portions of the southern cliff where past gravitational failures have left steep scarps [71]. These structures not only offer lateral resistance to shallow landslides but also allow for integration of vegetative reinforcement techniques, such as the insertion of willow cuttings or other regenerating species. Over time, the combination of structural support and root anchoring helps maintain slope stability while blending visually with the landscape.

Complementary to engineered containment is the promotion of native vegetation. Decades of afforestation with non-native, shallow-rooted species have contributed to hydrological imbalances and slope fragility [72]. Reintroducing deep-rooted Mediterranean species such as *Quercus ilex* (holm oak) and *Arbutus unedo* (strawberry tree), whose roots can reach depths of over 10 m, can significantly improve soil anchoring, reduce surface runoff, and counteract residual pore pressure build-up [73]. These botanical strategies must be guided by expert assessments to match species to micro-topographical and hydrological conditions. A gradual implementation plan, starting with the most unstable sectors, would enable progressive ecological stabilization.

Technological tools can further support slope monitoring. High-resolution LiDAR surveys and drone photogrammetry, repeated seasonally or post-event, would allow the detection of early-stage deformation, erosion, or regrowth patterns, creating a dynamic landslide inventory [74,75]. A network of corner reflectors and L-band DInSAR data would improve the monitoring of the ground movement by providing an improved measuring points density to distinguish the kinetic behavior of the different portion of the landsides [76]. Integrating these datasets with the piezometric and inclinometric network currently in place can enhance the predictive accuracy of early-warning thresholds.

However, physical mitigation alone is insufficient in such a socially dynamic system. The risk perception field survey highlighted that a large portion of visitors either underestimated or were unsure about the frequency of landslides, and that only one respondent knew about the civil protection plan. This lack of situational awareness calls for urgent investment in communication strategies. Rather than relying solely on top-down institutional messaging, communication efforts should prioritize simple, intuitive formats, directly embedded in tourists' experience [77]. Informational panels should be placed at strategic access points, featuring direct and accessible language, supported by visual cues (maps, danger icons, QR codes) [78], and adapted to different social groups. To avoid homogenized messaging, communication materials should be stratified by audience, for example using bolder colors and infographics for younger beachgoers, and longer explanatory text for older visitors.

In addition, hands-on seasonal briefings, such as on-site information sessions or simulations conducted with beach operators before summer openings, can foster community ownership of risk [79]. As beach concessionaires and service providers are the *de facto* first responders, they must be actively trained and involved in simulation exercises. Specific training content should include evacuation coordination, visual recognition of slope deformation signs, and real-time alert response protocols. Finally, a more accurate estimation of tourist inflows, particularly through the use of higher-resolution and temporally consistent remote sensing data combined with an expanded sample of surveyed visitors, would allow for a more precise spatial and temporal characterization of exposure. This, in turn, would improve the prioritization and contextualization of risk mitigation strategies during peak tourist periods. For instance, brochures distributed at tourism offices, translated into multiple languages, and embedded in practical platforms (e.g., shuttle bus tickets, tourist apps), can be a cost-effective complement to signage.

7.3. Broader implications for coastal risk management

This case study offers broader insights for the governance of geohydrological risks in tourist-oriented coastal settings, where physical exposure is high, but cognitive and procedural preparedness is low. This mismatch, clearly demonstrated by the fieldwork, challenges the conventional paradigms of civil protection, which tend to focus on stable, resident communities. In such contexts, emergency plans must evolve to reflect the socio-temporal fluidity of exposure. Tourist beaches like San Michele and Sassi Neri experience daily micro-cycles of crowding and dispersal, with a user base that changes every few hours and peaks during weekends or holidays. Consequently, risk communication must shift from long-term institutional channels to ephemeral, real-time tools. Mobile alerts triggered by meteorological or geological thresholds, trailhead beacons, or dynamic signage can ensure that even first-time visitors receive critical warnings in situ. These tools should be geo-located and multilingual, leveraging tourists' smartphones and habitual behaviors (e.g., scanning QR codes or checking shuttle schedules).

The analysis also reveals the limits of the current civil protection approach. When 99 % of users are unaware of existing evacuation plans, the real front line becomes the informal safety network: lifeguards, bar staff, and even fellow beachgoers. Their role must be redefined from passive bystanders to "recognized local safety actors". This requires formal integration into the emergency governance architecture, through agreements, seasonal protocols, and priority access to real-time updates.

Moreover, the example of Sirolo speaks to a larger planning gap: the invisibility of hazard in leisure landscapes. Tourists associate beaches with recreation, not risk. This cognitive dissonance hinders the uptake of warning messages or precautionary behavior. Risk communication, therefore, must adopt persuasive, affective strategies. Beyond technical signage, emotionally resonant messages, such as simulations of landslide scenarios or behavioral nudges, may be more effective at triggering protective action. To this end, collaborations with experts in behavioral science, environmental psychology, and user-centered design should be encouraged.

Eventually, the study demonstrates the broader need for adaptive civil protection planning that recognizes the transient nature of exposure in tourism-driven localities. As illustrated in Fig. 1, the workflow developed in this study and implemented for the Sirolo pilot case shows a flexible design that makes it potentially applicable to other coastal settings with comparable geological, geomorphological, and touristic conditions in the broader framework of climate change. In this condition, the Mediterranean basin itself is widely considered a climate change hotspot, with multiple studies projecting an increase in the frequency and intensity of extreme rainfall events. Such changes are likely to exacerbate slope instabilities in steep coastal settings, making integrated hazard–exposure–risk frameworks increasingly relevant for disaster risk reduction. Many coastal regions would benefit from adopting an integrative approach as the novel one proposed in this paper: coupling different geological disciplines with tourism social data and strengthening local actor readiness.

8. Conclusions

This study demonstrates how a multidisciplinary approach as the conceptual framework proposed in this study can effectively address both the physical drivers and societal dimensions of landslide risk in complex, high-exposure coastal settings. By combining detailed geomorphological and geological field mapping, multi-sensor monitoring (including DInSAR, inclinometers, and piezometers), rainfall trend analysis, and, we have developed a site-specific model of slope instability for the Sirolo coastline. Crucially, the inclusion of an innovative deep learning models to quantify seasonal tourist exposure and a structured risk perception survey among non-resident beach users has highlighted a significant gap between physical exposure and public awareness, underscoring the need for targeted communication and preparedness measures. We suggest a mitigation strategy which should follow an integrated, holistic path: combining slope stabilization, environmental regeneration, technological monitoring, and inclusive communication to match the seasonal rhythms and complexity of this iconic coastline.

Other Italian and international coastal destinations face similar hazards: steep cliffs, weak lithologies, and high tourist flows. The integrated approach piloted in this study, blending geomorphological diagnostics, environmental management, and social awareness, may offer a transferable model for coastal towns balancing natural beauty with latent geological threats. Managing landslide risk in tourist coasts requires a shift in logic: from resident-centric resilience to visitor-focused adaptability. Sirolo's experience shows that even modest investments in awareness, vegetation, and visibility can narrow the perception–exposure gap and lay the foundation for safer, more informed, and more sustainable coastal tourism. Future research should expand the quantitative understanding of visitor risk perception and behavior through larger seasonal surveys and explore the use of real-time monitoring and mobile-based early warning tools to reach transient populations. By continuing to integrate physical and social dimensions of hazard, coastal municipalities can better anticipate evolving risks and enhance the resilience of both landscapes and communities.

CRediT authorship contribution statement

Elisa Mammoliti: Writing – review & editing, Writing – original draft, Visualization, Validation, Methodology, Investigation, Formal analysis, Data curation. **Eleonora Gioia:** Writing – review & editing, Writing – original draft, Visualization, Validation, Methodology, Investigation, Formal analysis, Data curation, Conceptualization. **Davide Fronzi:** Writing – review & editing, Writing – original draft, Visualization, Validation, Methodology, Investigation, Formal analysis, Data curation. **Adriano Mancini:** Writing – original draft, Validation, Software, Investigation, Formal analysis, Data curation. **Giorgio Mattioli:** Visualization, Data curation. **Roberta Bonì:** Writing – original draft, Validation, Data curation. **Fabrizio Pontoni:** Methodology, Data curation, Conceptualization. **Stefano Marabini:** Methodology. **Stefano Mazzoli:** Methodology, Conceptualization. **Alberto Tazioli:** Supervision. **Alessandra Negri:** Writing – review & editing, Supervision, Resources, Project administration, Funding acquisition, Conceptualization.

Declaration of generative AI and AI-assisted technologies in the writing process

During the preparation of this work the authors used AI in order to improve language and readability. After using this tool, the authors reviewed and edited the content as needed and take full responsibility for the content of the publication.

Funding sources

This work was supported by the Cariverona Foundation under the 2024 Capitale Naturale program (CUP I53C24003730007).

Declaration of competing interest

The authors declare that they have no known competing financial interests or personal relationships that could have appeared to influence the work reported in this paper.

Acknowledgements

The authors would like to express their sincere gratitude to Professor Giuseppe Scarpelli and Professor Leonardo Cascini for their valuable advice throughout the development of this work. Authors also thank Ionita Amalia Elena for supporting risk perception analysis with her master's thesis. We warmly acknowledge little Lorenzo, who was present in his mother's womb (E.M.) and close to his father (D.F.) throughout the preparation and writing of this manuscript.

Data availability

Data will be made available on request.

References

[1] I. Alcántara-Ayala, Landslides in a changing world, Landslides (2025), https://doi.org/10.1007/s10346-024-02451-1.
[2] C. Violante, Rocky coast: geological constraints for hazard assessment, Geol. Soc. Lond. Spec. Publ. 322 (2009) 1–31, https://doi.org/10.1144/SP322.1.
[3] S. Qin, S. Wang, J.J. Jiao, A cusp catastrophe model of instability of slip-buckling slope, Rock Mech. Rock Eng. 34 (2001) 119–134, https://doi.org/10.1007/s006030170018.
[4] K.-T. Chang, L. Ge, H.-H. Lin, Slope creep behavior: observations and simulations, Environ. Earth Sci. 73 (2015) 275–287.
[5] M. Mantovani, S. Devoto, D. Piacentini, M. Prampolini, M. Soldati, A. Pasuto, Advanced SAR interferometric analysis to support geomorphological interpretation of slow-moving coastal landslides (Malta, Mediterranean Sea), Remote Sens. 8 (2016) 443, https://doi.org/10.3390/rs8060443.
[6] D. Piacentini, S. Devoto, M. Mantovani, A. Pasuto, M. Prampolini, M. Soldati, Landslide susceptibility modeling assisted by Persistent scatterers interferometry (PSI): an example from the northwestern coast of Malta, Nat. Hazards 78 (2015) 681–697.
[7] M. Della Seta, S. Martino, G.S. Mugnozza, Quaternary sea-level change and slope instability in coastal areas: insights from the Vasto Landslide (Adriatic coast, central Italy), Geomorphology 201 (2013) 462–478.
[8] F. Cotecchia, C. Vitone, F. Santaloia, G. Pedone, O. Bottiglieri, Slope instability processes in intensely fissured clays: case histories in the Southern Apennines, Landslides 12 (2015) 877–893.
[9] A. Aguzzoli, D. Arosio, M. Mulas, G. Ciccarese, B. Bayer, G. Winkler, F. Ronchetti, Multidisciplinary non-invasive investigations to develop a hydrogeological conceptual model supporting slope kinematics at Fontana Cornia landslide, Northern Apennines, Italy, Environ. Earth Sci. 81 (2022) 471.
[10] H.-E. Chen, Y.-Y. Chiu, T.-L. Tsai, J.-C. Yang, Effect of rainfall, runoff and infiltration processes on the stability of footslopes, Water 12 (2020) 1229, https://doi.org/10.3390/w12051229.
[11] F. Luino, J.V. De Graff, The Stava mudflow of 19 July 1985 (Northern Italy): a disaster that effective regulation might have prevented, Nat. Hazards Earth Syst. Sci. 12 (2012) 1029–1044.
[12] F. Ronchetti, L. Borgatti, F. Cervi, C. Gorgoni, L. Piccinini, V. Vincenzi, A. Corsini, Groundwater processes in a complex landslide, northern Apennines, Italy, Nat. Hazards Earth Syst. Sci. 9 (2009) 895–904.
[13] E. Mammoliti, D. Fronzi, S. Palpacelli, N. Biagiola, A. Tazioli, Assessment of urban landslide groundwater characteristics and origin using artificial tracers, hydro-chemical and stable isotope approaches, Environ. Earth Sci. 82 (2023) 211.
[14] United Nations Office for Disaster Risk Reduction (UNDRR), Sendai framework for disaster risk reduction 2015–2030 (Available from: https://www.undrr.org/publication/sendai-framework-disaster-risk-reduction-2015-2030, 2015.
[15] P. Bubeck, W.J.W. Botzen, J.C. Aerts, A review of risk perceptions and other factors that influence flood mitigation behavior, Risk Anal. Int. J. 32 (2012) 1481–1495.
[16] P. Slovic, Perception of Risk, vol. 236, Cited On, 1987, pp. 280–285, 207.
[17] M.K. Lindell, R.W. Perry, The protective action decision model: theoretical modifications and additional evidence, Risk Anal, Int. J. 32 (2012) 616–632.
[18] D. Bird, D. Dominey-Howes, Testing the use of a 'questionnaire survey instrument'to investigate public perceptions of tsunami hazard and risk in Sydney, Australia, Nat. Hazards 45 (2008) 99–122.
[19] L. Cugliari, A. Cerase, A. Amato, Tsunami risk perception, a state-of-the-art review with a focus in the NEAM region, Front. Earth Sci. 10 (2022) 995536.
[20] S.D. Park, J.G. Kim, W.H. Kim, H.S. Kim, Distribution of tritium in the leachates and methane gas condensates from municipal waste landfills in Korea, Water Environ. J. 19 (2005) 91–99, https://doi.org/10.1111/j.1747-6593.2005.tb00556.x.
[21] J. Rosselló, S. Becken, M. Santana-Gallego, The effects of natural disasters on international tourism: a global analysis, Tour. Manag. 79 (2020) 104080.
[22] H.M. Aucote, A. Miner, P. Dahlhaus, Interpretation and misinterpretation of warning signage: perceptions of rockfalls in a naturalistic setting, Psychol. Health Med. 17 (2012) 522–529.
[23] M. Shibata, Exploring international beachgoers' perceptions of safety signage on Australian beaches, Saf. Sci. 158 (2023) 105966.
[24] B. Matthews, R. Andronaco, A. Adams, Warning signs at beaches: do they work? Saf. Sci. 62 (2014) 312–318.
[25] D.M. Kennedy, S. Sherker, B. Brighton, A. Weir, C.D. Woodroffe, Rocky coast hazards and public safety: moving beyond the beach in coastal risk management, Ocean Coast Manag. 82 (2013) 85–94.
[26] A.M. Gstaettner, D. Lee, K. Rodger, The concept of risk in nature-based tourism and recreation– a systematic literature review, Curr. Issues Tourism 21 (2018) 1784–1809.
[27] W. Koon, A. Peden, J.C. Lawes, R.W. Brander, Coastal drowning: a scoping review of burden, risk factors, and prevention strategies, PLoS One 16 (2021) e0246034.
[28] S. Becken, K.F. Hughey, Linking tourism into emergency management structures to enhance disaster risk reduction, Tour. Manag. 36 (2013) 77–85.
[29] ISTAT, Resident population in Sirolo, year 2023. https://esploradati.istat.it/databrowser/#/it/dw/categories/IT1,POP,1.0/POP_POPULATION/DCIS_POPRES1/DCIS_POPRES1_REG_MUN/IT1,22_289_DF_DCIS_POPRES1_14,1.0, 2024. (Accessed 9 July 2025).
[30] Marche Region, Arrivi e presenze totali per tipo di esercizio, comune e provincia delle Marche - Anno 2022, 2024, https://statistica.regione.marche.it/Marche-in-Numeri/Turismo, 2023. (Accessed 9 July 2025).
[31] A. Trigila Apat, Rapporto Sulle Frane in Italia: Il Progetto IFFI: Metodologia, Risultati E Rapporti Regionali, APAT, 2007.
[32] C. Reis, M. Lopes, M.A. Baptista, S. Clain, Towards an integrated framework for the risk assessment of coastal structures exposed to earthquake and tsunami hazards, Resil. Cities Struct. 1 (2022) 57–75.
[33] E. Laino, I. Toledo, L. Aragonés, G. Iglesias, A novel multi-hazard risk assessment framework for coastal cities under climate change, Sci. Total Environ. 954 (2024) 176638.
[34] L. Sangelantoni, E. Gioia, F. Marincioni, Impact of climate change on landslides frequency: the Esino river basin case study (Central Italy), Nat. Hazards 93 (2018) 849–884.
[35] F.M. Calafat, T. Frederikse, K. Horsburgh, The sources of sea-level changes in the Mediterranean Sea since 1960, J. Geophys. Res. Oceans 127 (2022) e2022JC019061.
[36] G. Lazoglou, A. Papadopoulos-Zachos, P. Georgiades, G. Zittis, K. Velikou, E.M. Manios, C. Anagnostopoulou, Identification of climate change hotspots in the Mediterranean, Sci. Rep. 14 (2024) 29817.
[37] D. Aringoli, B. Gentili, M. Materazzi, G. Pambianchi, P. Farabollini, Il Ruolo Della Gravità Nell'Evoluzione Geomorfologica Di Un'Area Di Falesia: Il Caso Del Monte Conero (Mare Adriatico, Italia Centrale), 2014, p. 14.
[38] A. Montanari, P. Sandroni, Le Rocce Del Conero Raccontano: Una Breve Guida Geoescursionistica, Parco Del Conero (IS), 1995.
[39] M. Coltorti, T. Nanni, M.L. Rainone, Il contributo delle scienze della terra nell'elaborazione di un piano paesistico: l'esempio del Monte Conero (Marche), Mem Soc Geol It 37 (1987) 629–647.

[40] G. Cello, L. Coppola, Modalità e stili deformativi nell'area anconetana, Stud. Geol. Camerti 11 (1989) 37–47.
[41] L. Chemeri, M. Taussi, D. Fronzi, J. Cabassi, S. Mazzoli, A. Tazioli, A. Renzulli, O. Vaselli, Groundwater hydrogeochemical changes predating and following the November 9, 2022 Mw 5.5 Adriatic offshore earthquake (central Italy), J. Hydrol. (2025) 132792.
[42] M. De Donatis, S. Mazzoli, F.-C. Wezel, Evoluzione tettonica dell'avanfossa appenninica marchigiano-romagnola dal Miocene superiore al Pleistocene, Studi Geol. Camerti. Vol. Spec. 1995 (1996) 359–371.
[43] L. Marchegiani, G. Deiana, E. Tondi, Tettonica pre-orogenica in Appennino centrale, Stud. Geol. Camerti Nuova Ser. 14 (1999) 211–228.
[44] V.M.E. Fruzzetti, D. Segato, P. Ruggeri, A. Vita, E. Sakellariadi, G. Scarpelli, Fenomeni Di Instabilità Della Falesia Del Monte Conero: Ruolo Dell'Assetto Strutturale, 2011, p. 6.
[45] D. Fronzi, F. Banzato, S. Caliro, C. Cambi, C. Cardellini, R. Checcucci, L. Mastrorillo, F. Mirabella, P. Marco, D. Valigi, Preliminary results on the response of some springs of the Sibillini Mountains area to the 2016-2017 seismic sequence, ACQUE Sotter 9 (2020) 19–25.
[46] D. Valigi, D. Fronzi, C. Cambi, G. Beddini, C. Cardellini, R. Checcucci, L. Mastrorillo, F. Mirabella, A. Tazioli, Earthquake-Induced Spring Discharge Modifications: the Pescara di Arquata Spring Reaction to the August–October 2016 Central Italy Earthquakes, Water 12 (2020) 767, https://doi.org/10.3390/w12030767.
[47] G. Mattioli, D. Fronzi, E. Mammoliti, A. Tazioli, Assessing groundwater depletion in a changing climate through the vadose zone monitoring and a novel extreme rainfall index, oral presentation at Flowpath- National Meeting on Hydrogeology, June 2025, pp. 11–13. Torino, Italy.
[48] M.M. Monir, M. Rokonuzzaman, S.C. Sarker, E. Alam, M.K. Islam, A.R.M.T. Islam, Spatiotemporal analysis and predicting rainfall trends in a tropical monsoon-dominated country using MAKESENS and machine learning techniques, Sci. Rep. 13 (2023) 13933.
[49] E. Romano, A.B. Petrangeli, F. Salerno, N. Guyennon, Do recent meteorological drought events in central Italy result from long-term trend or increasing variability? Int. J. Climatol. 42 (2022) 4111–4128.
[50] D. Fronzi, M. Gaiolini, E. Mammoliti, N. Colombani, S. Palpacelli, M. Marcellini, A. Tazioli, Groundwater-surface water interaction revealed by meteorological trends and groundwater fluctuations on stream water level, Acque Sotter.-Ital. J. Groundw. 11 (2022) 19–28.
[51] D. Fronzi, G. Narang, A. Galdelli, A. Pepi, A. Mancini, A. Tazioli, Towards groundwater-level prediction using prophet forecasting method by exploiting a high-resolution hydrogeological monitoring system, Water 16 (2024) 152.
[52] J.C. García-Davalillo, G. Herrera, D. Notti, T. Strozzi, I. Álvarez-Fernández, DInSAR analysis of ALOS PALSAR images for the assessment of very slow landslides: the Tena Valley case study, Landslides 11 (2014) 225–246.
[53] S. Morelli, R. Bonì, M. De Donatis, L. Marino, G.F. Pappafico, M. Francioni, A low-cost and fast operational procedure to identify potential slope instabilities in cultural Heritage sites, Remote Sens. 15 (2023) 5574.
[54] D. Di Martire, M. Paci, P. Confuorto, S. Costabile, F. Guastaferro, A. Verta, D. Calcaterra, A nation-wide system for landslide mapping and risk management in Italy: the second not-ordinary Plan of environmental Remote sensing, Int. J. Appl. Earth Obs. Geoinformation 63 (2017) 143–157.
[55] A. Ferretti, C. Prati, F. Rocca, Permanent scatterers in SAR interferometry, IEEE Trans. Geosci. Rem. Sens. 39 (2002) 8–20.
[56] M. Costantini, S. Falco, F. Malvarosa, F. Minati, A new method for identification and analysis of persistent scatterers in series of SAR images, in: IGARSS 2008-2008 IEEE Int. Geosci. Remote Sens. Symp., IEEE, 2008. II-449-II–452.
[57] M. Crosetto, B. Crippa, M. Mróz, M. Cuevas-González, S. Shahbazi, Applications based on EGMS products: a review, Remote Sens. Appl. Soc. Environ. (2025) 101452.
[58] Larsen, Y.; Marinkovic, P.; Dehls, J.; Stødle, D, End user interface manual., (n.d.). Available online: https://land.copernicus.eu/usercorner/technical-library/egms-end-user-interface-manual.
[59] R. Bonì, M. Bordoni, V. Vivaldi, C. Troisi, M. Tararbra, L. Lanteri, F. Zucca, C. Meisina, Assessment of the Sentinel-1 based ground motion data feasibility for large scale landslide monitoring, Landslides 17 (2020) 2287–2299.
[60] R. Khanam, M. Hussain, Yolov11: an Overview of the Key Architectural Enhancements. Arxiv, ArXiv Prepr. ArXiv241017725, 2024 n.d.
[61] Marche Region, Arrivi e presenze totali per tipo di esercizio, comune e provincia delle Marche - Anno 2022, n.d. https://statistica.regione.marche.it/Marche-in-Numeri/Turismo, 2023.
[62] W.G. Cochran, Sampling Techniques, john wiley & sons, 1977.
[63] M. Shin, J. Jeong, Optimistic bias: concept analysis, Res. Community Public Health Nurs. 35 (2024) 112–123.
[64] F. Cui, Y. Liu, Y. Chang, J. Duan, J. Li, An overview of tourism risk perception, Nat. Hazards 82 (2016) 643–658.
[65] X. Li, Y. Chen, A.L. Handwerger, G. Buscarnera, Dynamics of creeping landslides controlled by inelastic hydro-mechanical couplings, Eng. Geol. 317 (2023) 107078, https://doi.org/10.1016/j.enggeo.2023.107078.
[66] F. Troiani, S. Martino, G.M. Marmoni, M. Menichetti, D. Torre, G. Iacobucci, D. Piacentini, Integrated field surveying and land surface quantitative analysis to assess landslide proneness in the Conero promontory rocky Coast (Italy), Appl. Sci. 10 (2020) 4793.
[67] G.M. Marmoni, S. Martino, M. Censi, M. Menichetti, D. Piacentini, G. Scarascia Mugnozza, D. Torre, F. Troiani, Transition from rock mass creep to progressive failure for rockslide initiation at mt. Conero (Italy), Geomorphology 437 (2023) 108750, https://doi.org/10.1016/j.geomorph.2023.108750.
[68] F.E. Maesano, M. Buttinelli, R. Maffucci, G. Toscani, R. Basili, L. Bonini, P. Burrato, J. Fedorik, U. Fracassi, Y. Panara, Buried alive: imaging the 9 November 2022, Mw 5.5 earthquake source on the offshore Adriatic blind thrust front of the Northern Apennines (Italy), Geophys. Res. Lett. 50 (2023) e2022GL102299.
[69] G. Pezzo, A. Billi, E. Carminati, A. Conti, P. De Gori, R. Devoti, F.P. Lucente, M. Palano, L. Petracchini, E. Serpelloni, Seismic source identification of the 9 November 2022 Mw 5.5 offshore Adriatic sea (Italy) earthquake from GNSS data and aftershock relocation, Sci. Rep. 13 (2023) 11474.
[70] A. Montanari, M. Mainiero, R. Coccioni, G. Pignocchi, Catastrophic landslide of medieval Portonovo (Ancona, Italy), Geol. Soc. Am. Bull. 128 (2016) 1660–1678, https://doi.org/10.1130/B31472.1.
[71] F. Preti, C. Crocetti, S. Nijimbere, J.M.V. Nsabiyumva, C. Hicintuka, G. Castelli, Soil and Water Bioengineering (SWBE) in Africa: first experience and lessons-learned in Burundi, Ecol. Eng. 212 (2025) 107510.
[72] Ente Parco Regionale del Conero, Naturalistic management plan of the conero Park, n.d. https://www.parcodelconero.org/wp-content/uploads/Piano-Gest-Natural/Piano-di-Gestione-Naturalistica-del-Parco-del-Conero.pdf (accessed July 9, 2025).
[73] E. Biondi, The Vegetation of Mount Conero (With Vegetation Map at 1:10,000 Scale), Regione Marche, 1986.
[74] J. Sun, G. Yuan, L. Song, H. Zhang, Unmanned aerial vehicles (UAVs) in landslide investigation and monitoring: a review, Drones 8 (2024) 30.
[75] P. Sestras, G. Badea, A.C. Badea, T. Salagean, V.-E. Oniga, S. Roşca, Ştefan Bilaşco, S. Bruma, V. Spalević, S. Kader, A novel method for landslide deformation monitoring by fusing UAV photogrammetry and LiDAR data based on each sensor's mapping advantage in regards to terrain feature, Eng. Geol. 346 (2025) 107890.
[76] T. Smail, M. Abed, A. Mebarki, M. Lazecky, Earthquake-induced landslides monitoring and survey by means of InSAR, Nat. Hazards Earth Syst. Sci. Discuss. 2021 (2021) 1–16.
[77] A. Cui, J. Fountain, S. Espiner, Communicating natural hazard risks to Chinese visitors: a case study from New Zealand, Front. Sustain. Tour. 2 (2023) 1192124.
[78] V. Meyer, C. Kuhlicke, J. Luther, S. Fuchs, S. Priest, W. Dorner, K. Serrhini, J. Pardoe, S. McCarthy, J. Seidel, Recommendations for the user-specific enhancement of flood maps, Nat. Hazards Earth Syst. Sci. 12 (2012) 1701–1716.
[79] S.P. Leatherman, S.B. Leatherman, N. Rangel-Buitrago, Integrated strategies for management and mitigation of beach accidents, Ocean Coast Manag. 253 (2024) 107173.